MILPNET: A MULTI-SCALE ARCHITECTURE WITH GEOMETRIC FEATURE SEQUENCE REPRESENTATIONS FOR ADVANCING MILP PROBLEMS

Anonymous authors
Paper under double-blind review

ABSTRACT

We propose *MILPnet*, a multi-scale hybrid attention framework that models Mixed Integer Linear Programming (MILP) problems as geometric sequences rather than graphs. This approach directly addresses the challenge of Foldable MILP instances, a class of problems that graph-based models, specifically Graph Neural Networks (GNNs), fail to distinguish due to expressiveness limits imposed by the Weisfeiler-Lehman test. By representing MILPs through sequences of constraint and objective features, *MILPnet* captures both local and global geometric structure using a theoretically grounded multi-scale attention mechanism. We theoretically prove that *MILPnet* can approximate feasibility, optimal objective value, and optimal solution mappings over a measurable topological space with arbitrarily small error. Empirically, *MILPnet* outperforms graph-based methods by multiple orders of magnitude in feasibility prediction accuracy and convergence speed on Foldable MILPs, while using significantly fewer parameters. It also generalizes effectively across problem scales and demonstrates strong performance on real-world MILP benchmarks when integrated into an end-to-end solver pipeline. Our code is available with the `https://anonymous.4open.science/r/MILPnet-2BD1/`.

1 INTRODUCTION

Mixed-integer linear programming (MILP) is a foundational combinatorial optimization problem characterized by a linear objective function and linear constraints, with decision variables that can be either continuous or discrete. This flexibility makes MILP highly expressive and applicable in diverse real-world domains, such as transportation systems (Goldman & Trevisan, 2023; Wang et al., 2023a), route optimization (Mammeri, 2019; Chen et al., 2023a), and power system planning (Zhang et al., 2020; Chen et al., 2024).

However, as a well-known NP-hard problem, solving MILP remains a significant challenge. Traditional methods, such as Branch-and-Bound (Land & Doig, 1960) and Cutting Planes (Gomory, 1958), are commonly employed but become impractical for large-scale instances due to their intensive resource requirements.

Recently, Machine Learning methods have emerged as a promising alternative. ML models can approximate solutions efficiently by leveraging the implicit structure and patterns within MILP problems and integrating them with reinforcement learning or MILP Exact solvers. These approaches can significantly reduce computational costs while delivering effective solutions within practical timeframes (Bengio et al., 2018; tian Wu & min Yang, 2022; Wang et al., 2023a; 2024). Generative models, including diffusion models, have also been explored for solving structured MILP variants, such as the Traveling Salesman Problem (TSP) and the Maximum Independent Set Problem (MIS) (Sun & Yang, 2023; Sanokowski et al., 2024; Ma et al., 2024), showing strong performance and generalization.

A recent trend has been to solve MILPs using Graph Neural Networks (GNNs), treating MILP instances as bipartite graphs that link variables and constraints (Han et al., 2023; Ye et al., 2023; Paulus & Krause, 2023a; Geng et al., 2024). However, Bipartite graphs and GNNs can capture relationships between constraints and variables, missing the interactions between the constraints themselves, which potentially contain crucial features, such as feasible regions or optimal solutions of

the MILP. Thus, GNN-based solutions suffer from a fundamental limitation: **they cannot distinguish between non-isomorphic MILP instances that differ in feasibility**, due to the expressive bounds of the Weisfeiler-Lehman (WL) test. As shown in recent work (Chen et al., 2023b), this leads to failure cases known as **Foldable MILP**s, where multiple distinct MILP instances are indistinguishable to GNNs but differ critically in their feasible regions.

Although, recent research (Chen et al., 2023b) partially addresses this by injecting random features into graph structures. However, they only bypass WL-test limitations without capturing fundamental characteristics of MILP instances themselves. Current graph-based models remain inadequate for robust feasibility prediction and high-fidelity representation of general MILP problems, especially Foldable MILPs.

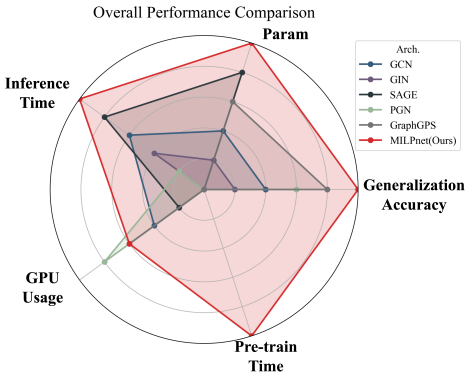

Figure 1: Overall performance comparison between MILPnet and graph-based models. **Larger area indicates better performance.**

To overcome these limitations, we propose a novel representation framework that departs from the graph paradigm and instead adopts a computational geometry perspective. Considering the geometric and topological uniqueness of MILP problems (Huchette & Vielma, 2019; Conforti et al., 2010), we encode each MILP instance by extracting spatial geometric feature vectors, including hyperplane vectors from linear constraints, discrete integer point features, and direction vector from the linear objective function, and assemble these into a sequence. To the best of our knowledge, this is the first work to represent MILPs as sequences.

Given the complexity of MILP problems, we propose a Multi-Scale Hybrid Attention mechanism that enables our model, MILPnet, to learn both local and global features from the MILP sequence. Furthermore, we mathematically prove that our model can effectively approximate the feature mappings of any MILP instance with arbitrarily small error.

We validated our approach on Foldable MILP instances, which are specifically challenging for GNN- and Graph-based models. Across feasibility, optimal solution, and optimal object value predictions, MILPnet achieves improvements of multiple orders of magnitude in accuracy and convergence speed, while using significantly fewer parameters and pre-training time. As summarized in Figure 1, MILPnet consistently outperforms baseline models across five key dimensions: generalization, accuracy, model size, inference time, and GPU memory usage. These results highlight the effectiveness of our geometric modeling and its broad potential.

2 Related Work

MILP is a classic NP-hard problem. Traditional methods, such as branch-and-bound (Gomory, 1958) and cut-plane methods (Land & Doig, 1960), typically solve MILPs by simplifying or relaxing the problem. However, these methods can incur exponential time complexity in the worst case, limiting their scalability for large or real-time applications.

To address these challenges, machine learning methods have been applied to accelerate the MILP solving process. Specifically, most methods model MILP instances with GNNs, framing them as weighted bipartite graphs (Gupta et al., 2020). These graphs typically consist of two disjoint sets of nodes: variables and constraints. Message-passing mechanisms within GNNs are then used to capture their structural relationships. Notable ML-based methods include diffusion-model-based MILP solvers (Sun & Yang, 2023; Yu et al., 2024; Sanokowski et al., 2024), predict and search frameworks (Han et al., 2023; Huang et al., 2023), hybrid approaches that combine GNNs with reinforcement learning or traditional solving techniques (Wang et al., 2023a), and heuristic algorithms (He et al., 2014; Gasse et al., 2019; Chmiela et al., 2021; Paulus & Krause, 2023a).

Formally, a bipartite graph is denoted as $G = (V \cup W, E)$, where V and W represent the variable and constraint nodes, respectively. The set $G_{m,n}$ includes all such graphs with $|V| = m$ and

$|W| = n$, while the complete graph representation with node features for an MILP is given by $(G, H) \in G_{m,n} \times H_m^V \times H_n^W$.

While these graph-based models are effective in capturing variable-constraint relationships, they inherently miss higher-order interactions, particularly between constraints themselves, which may encode crucial information about feasibility or optimality. Therefore, for a class of MILP instances known as **Foldable MILP**s (Theorem 2.1), GNN-based models cannot represent their feasibility as the underlying WL-test cannot distinguish non-isomorphic graphs. Conversely, MILP instances that are not Foldable MILPs are Unfoldable MILPs.

Theorem 1. *(Lemma 3.2. in (Chen et al., 2023b)) There exist two MILP problems (G, H) and $(G, \hat{H})$, with one being feasible and the other one being infeasible, such that $(G, H) \sim (G, \hat{H})$.*

This finding underscores a critical gap: graph-based models, regardless of feature augmentation, fundamentally cannot resolve the feasibility of Foldable MILP instances. It signifies the need for alternative representations beyond graph-based modeling to enhance the feasibility prediction for complex MILP problems.

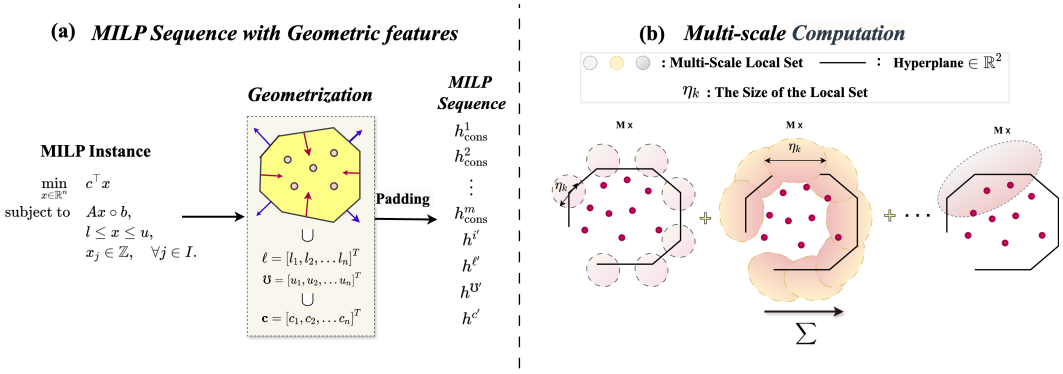

Figure 2: Overview of MILPnet. (a) An MILP instance is transformed into a sequence of geometric feature tokens, including constraint hyperplanes, variable bounds, integer indicators, and the objective vector. (b) The sequence is processed by a multi-scale hybrid attention architecture, enabling accurate approximation of feasibility, optimal objective value, and solution mappings.

3 Preliminaries

MILP formulation. MILP is an NP-hard optimization problem characterized by a linear objective function and a set of linear constraints, with a subset of variables restricted to integer values. The standard formulation is:

$$\min_{x \in \mathbb{R}^n} c^\top x \quad \text{s.t.} \quad Ax \circ b, \quad l \le x \le u, \quad x_j \in \mathbb{Z}\ \forall j \in I \tag{1}$$

where $A \in \mathbb{R}^{m \times n}$, $b \in \mathbb{R}^m$, and $c \in \mathbb{R}^n$ are the problem parameters, $l, u \in (\mathbb{R} \cup \{\pm\infty\})^n$ specifies the variable bounds, $\circ \in \{\le, =, \ge\}^m$ denotes the constraint types, and $I \subseteq \{1, \dots, n\}$ indexes the variables that are required to be integer.

Feasibility. From a geometric perspective, define the continuous feasible region as a polyhedron $P = \{\, x \in \mathbb{R}^n \mid A\, x \circ b,\ l \le x \le u\}$ and the integer lattice as $\mathbb{Z}_I^n = \{\, x \in \mathbb{R}^n \mid x_j \in \mathbb{Z},\ \forall j \in I\}$. The MILP feasible set is their intersection $S = P \cap \mathbb{Z}_I^n$, i.e. all points that satisfy the linear constraints and bounds while taking integer values in the specified dimensions. If $S = \emptyset$, the MILP is infeasible.

Optimal solution and optimal objective value. A point $x^* \in S$ is called an **optimal solution** if it minimizes the objective function over all feasible points: $c^\top x^* \le c^\top x, \forall x \in S$. The corresponding scalar $c^\top x^*$ is the **optimal objective value**. If the objective can be decreased arbitrarily, i.e., for any $\epsilon > 0$, there exists $\hat{x} \in S$ such that $c^\top \hat{x} < -\epsilon$, the MILP is unbounded and the optimal value is $-\infty$.

4 SEQUENCE MODELING FOR MILP: MILP-SEQUENCE

This section introduces the first component of MILPnet (Figure 2 (a)), which encodes an MILP instance into a sequence representation from a geometric perspective. The MILP instance is decomposed into multiple components, each modeled in a well-defined topological space, forming what we refer to as the MILP-sequence.

4.1 GEOMETRIC MODELING OF MILP

We first reformulate the MILP problem from a geometric perspective. The MILP space consists of high-dimensional hyperplanes or half-spaces (from linear constraints and variable bounds), discrete point sets (from integrality requirements), and a direction vector (from the objective function). Together, these are represented as $P_{\text{constraint}} \cup P_{\text{range}} \cup I \cup c$. Each of these components is defined within a topological space as follows:

Linear constraints. The linear constraints are represented as the union of hyperplanes: $P_{\text{constraint}} = \bigcup_{i=1}^{m} H_i$, where H_i is the i-th hyperplane or half-space defined by the vector $h^i_{cons} = (n_i, d_i, b_i)$, where $n_i \in \mathbb{R}^n$ is the normal vector of H_i, $d_i \in \{-1, 0, 1\}$ denotes its directional type, and $b_i \in \mathbb{R}$ is the bias term. h_i is chosen from the topological space $H^{\text{cons}} = (\mathbb{R}^n) \times \{-1, 0, 1\} \times \mathbb{R}$.

Variable bounds. The bounds on variables define upper and lower half-spaces: $P_{\text{range}} = \left(\bigcup_{j=1}^{n} H_{\text{upper},j}\right) \bigcup \left(\bigcup_{j=1}^{n} H_{\text{lower},j}\right)$, where$H_{\text{upper},j} = \{x \in \mathbb{R}^n \mid x_j \leq u_j\}$ and $H_{\text{lower},j} = \{x \in \mathbb{R}^n \mid x_j \geq l_j\}$. We encode the bounds as vectors $h^{\ell} = (l_1, l_2, \ldots, l_n)$ and $h^{\mho} = (u_1, u_2, \ldots, u_n)$, drawn from the topological spaces $L = \prod_{j=1}^{n} L_i \subset \mathbb{R}^n$ and $U = \prod_{j=1}^{n} U_i \subset \mathbb{R}^n$, respectively, each equipped with the standard Euclidean topology. $\prod$ denotes the Cartesian product. The combined vector $\ell \cup \mho$ belongs to the space $H^{\text{Var}} = \mathbb{R}^{2n}$.

Integer set. The integrality constraints are encoded using a binary vector: $h^i = (i_1, i_2, i_3, \ldots, i_n) \in \{0, 1\}^n$, where $i_k = 1$ if x_k is constrained to be an integer, and $i_k = 0$ otherwise. This vector resides in the discrete topological space $I = \{0, 1\}^n$.

Linear optimization direction. The objective function is represented by a coefficient vector $h^c = (c_1, c_2, \ldots, c_n) \in \mathbb{R}^n$, drawn from the topological space $H^{\text{obj}} = \mathbb{R}^n$.

It is worth noting that, although the MILP feasible region is mathematically defined by intersections, we use unions in our geometric reformulation to denote the collection of individual components (e.g., constraint hyperplanes and bounds) treated as sequence tokens. This formulation expands the representational space, enabling MILPnet to more effectively explore the solution structure and approximate optimal outcomes.

4.2 MEASURES OF THE MILP GEOMETRIC SPACES

To unify component representations and manage dimensionality differences, we apply zero-padding, yielding two related topological spaces H^{MILP0} (original) and H^{MILP} (padded). The padded component spaces include $H^{\text{cons}}, H^{\text{Var}'}, H^{\text{obj}'}, I'$. As shown in Theorem 5 in Appendix, the spaces padded and non-padded are homeomorphic, ensuring no representation loss.

Measures. We equip each continuous space $(\mathbb{R}^n, \mathbb{R}^{2n}, \mathbb{R})$ with Borel σ-algebra and Lebesgue measure, and each discrete component $(\{-1, 0, 1\}, \{0\}, \{0, 1\}^n)$ with the counting measure. By product construction, the component measures are $\mu_{H^{\text{cons}}} = \lambda_{\mathbb{R}^n} \times \mu_{\{-1,0,1\}} \times \lambda_{\mathbb{R}}$, $\mu_{H^{\text{Var}'}} = \lambda_{\mathbb{R}^{2n}} \times \mu^4_{\{0\}}$, $\mu_{H^{\text{obj}'}} = \lambda_{\mathbb{R}^n} \times \mu^2_{\{0\}}$, $\mu_{I'} = \mu_{\{0,1\}^n} \times \mu^2_{\{0\}}$. The overall padded topological space is $H^{\text{MILP}} = ((H^{\text{cons}})^m \cup H^{\text{Var}'}) \times I' \times H^{\text{obj}'}$, which is measurable by construction.

4.3 GEOMETRIC FEATURE INTEGRATION

We now integrate the MILP geometric feature vectors into a sequence-based representation, treating each feature vector as a token.

MILP-sequence. Since the linear constraints h^i_{cons}, integer point sets $h^{i'}$, and variable ranges $h^{\ell'}$ and $h^{\mho'}$ are permutation invariant (as formalized in Theorems 6 and 7 in Appendix), we can arrange

them in any order. To preserve this invariance and recognize the term objective function's unique role, we place the objective token $h^{c'}$ at the end of the sequence. Thus, the MILP-sequence is:

$$\mathbf{x} = [h^1_{\text{cons}}, h^2_{\text{cons}}, \ldots, h^m_{\text{cons}}, h^{i'}, h^{\ell'}, h^{\mathfrak{V}'}, h^{c'}], \quad h \in \mathbb{R}^{n+2} \tag{2}$$

The topological space corresponding to the MILP-sequence is defined as $H^{\text{MILP}} \subset \mathbb{R}^{(m+4)(n+2)}$.

Sequence-based mappings. With this representation, we define the core mappings used to analyze MILP instances: **Feasibility mapping** $\Phi_{\text{feas}} : H^{\text{MILP}} \to \{0, 1\}$, **Optimal objective value mapping** $\Phi_{\text{obj}} : H^{\text{MILP}} \to \mathbb{R} \cup \{\infty, -\infty\}$, and **Optimal solution mapping** $\Phi_{\text{solu}} : \widetilde{H}^{\text{MILP}} \cap \Phi^{-1}_{\text{feas}}(1) \to \mathbb{R}^n$. These mappings are formally defined in Definitions 8 to 10 in the Appendix. We prove their measurability in Appendix G.

5 Multi-Scale Hybrid Attention for MILP-sequence

This section introduces the second core component of MILPnet (Figure 2 (b)): a novel Multi-Scale Hybrid Attention mechanism specifically designed to model MILP sequences. This architecture enables the network to capture both fine-grained local structure and global context by combining multiple levels of attention. It operates directly on the MILP-sequence defined in the previous section and is supported by a rigorous approximation theory over the measurable space H^{MILP}.

5.1 Shifted-Window Multi-Scale Attention

The geometric structure of MILPs suggests that relationships among constraints can reflect topological characteristics of the feasible region. To leverage this structure, we employ multi-scale local attention via sliding windows that extract features from various neighborhoods in the MILP-sequence.

Shifted-Window Local Attention. Given an embedded MILP-sequence $\mathbf{X}_{\text{embed}} \in \mathbb{R}^{(m+4)\times(n+2)}$, derived through linear projection, we define local attention windows that slide across the sequence. For each token at position $i \in \{1, \ldots, m+4\}$, a window of size η_k is centered at i, covering elements from position $i_{\min} = \max(i - \lfloor \frac{\eta_k - 1}{2} \rfloor, 1)$ to position $i_{\max} = \min(i + \lceil \frac{\eta_k - 1}{2} \rceil - 1, m + 4)$. To effectively capture the relationship between multi-level features and the MILP's overall goal, this window also needs to incorporate the embedding of the objective function feature $h^{c'}$ at position $m + 4$. Therefore, the position indices $\eta_k(i)$ for the window attention at position i with the window size η_k are defined as:

$$\eta_k(i) = \{j \in [i_{\min}, i_{\max}]\} \cup \{m + 4\}. \tag{3}$$

Then, the local attention at position i for scale η_k is computed as:

$$\mathbf{Q}^{\eta_k}_i = \mathbf{W}_Q \mathbf{X}_{\text{embed},i}, \mathbf{K}^{\eta_k}_j = \mathbf{W}_K \mathbf{X}_{\text{embed},j}, \mathbf{V}^{\eta_k}_j = \mathbf{W}_V \mathbf{X}_{\text{embed},j}, \quad j \in \eta_k(i) \tag{4}$$

$$\alpha^{\eta_k}_{ij} = \text{softmax}\left(\frac{\mathbf{Q}^{\eta_k}_i \cdot (\mathbf{K}^{\eta_k}_j)^\top}{\sqrt{d_k}}\right), \quad j \in \eta_k(i), \quad \mathbf{Att}^{\eta_k}_i = \sum_{j \in \eta_k(i)} \alpha^{\eta_k}_{ij} \mathbf{V}^{\eta_k}_j \tag{5}$$

where $\mathbf{W}_Q$, $\mathbf{W}_K$, $\mathbf{W}_V$ are the linear transformation matrices for Query, Key, and Value, and d_k is the dimension of the key vectors, which is split from the embedding size d_{dim} by the multi-heads. softmax function is used to normalize the Attention weights.

Multi-Scale MILP-sequence Attention. To aggregate information at different granularities, we apply local attention using N window sizes. The resulting outputs are averaged to produce the multi-scale representation,which is like the style in the Figure 2 (b).

$$\mathbf{Att}^{\text{multi}} = \frac{1}{N} \sum_{i=1}^{m+4} \sum_{k=1}^{N} \mathbf{Att}^{\eta_k}_i = \frac{1}{N} \sum_{k=1}^{N} \sum_{i=1}^{m+4} \left(\sum_{j \in \eta_k(i)} \alpha^{\eta_k}_{ij} \mathbf{V}^{\eta_k}_j \right) \tag{6}$$

where window sizes $\eta_k \in [2, m + 4]$ allow for a comprehensive evaluation of local and global contextual influences. Let $\eta_{\max} = \max_k(\eta_k)$ denote the largest window size.

Hybrid Attention Integration. To capture both multi-scale locality and global context, we define a hybrid attention mechanism that integrates multi-scale attention with global attention using a learnable parameter α:

$$\mathbf{Att}^{\text{hybrid}} = \alpha \cdot \mathbf{Att}^{\text{multi}} + (1 - \alpha) \cdot \mathbf{Att}^{\text{global}} \tag{7}$$

As illustrated in Figure 2, each MILP instance is first geometrically encoded as a feature vector in $\mathbb{R}^{n+2}$, and then padded to form an MILP-sequence of length $m+4$. This sequence undergoes linear projection and position encoding to produce the embedded input:$\mathbf{z} = [\mathrm{z}_1, \mathrm{z}_2, ..., \mathrm{z}_{n+2}] + \mathbf{z}_{\text{position}}$. With this embedded sequence, MILPnet applies its Hybrid Attention (HYA) mechanism, followed by residual connections and layer normalization. The computation at the l-th layer proceeds as:

$$\hat{\mathbf{z}}^l = \mathrm{HYA}(\mathrm{LN}(\mathbf{z}^{l-1}) + \mathbf{z}^{l-1}), \mathbf{z}^l = \mathrm{MLP}(\mathrm{LN}(\hat{\mathbf{z}}^l) + \hat{\mathbf{z}}^l) \tag{8}$$

where LN denotes layer norm, MLP refers to a position-wise feedforward network. Detailed information is in Figure 6 from Appendix.

Time Complexity. The computational complexity of the hybrid attention is $O\big(h\,d\,(m+4)^2\,(N+1)\big)$ where h is the number of attention heads, d is the embedding size, m is the number of the constraints, and N is the number of windows. Detailed analysis is provided in Appendix I.

5.2 MILPnet Representation on the Measurable Space H^{MILP}

We now formally demonstrate that the multi-scale hybrid architecture of MILPnet is capable of approximating the feature mappings of any MILP instance, when represented as a sequence in the measurable topological space H^{MILP}. We define two function classes: $\mathcal{F}^{\mathrm{MILP}}_{\mathrm{HYA}}\colon H^{\mathrm{MILP}} \to \mathbb{R}$ for scalar-valued network mappings, and $\mathcal{F}^{\mathrm{MILP}}_{\mathrm{HYA,V}}\colon H^{\mathrm{MILP}} \to \mathbb{R}^n$ for vector-valued network mappings with fixed output dimension n. By leveraging these mappings and the measurability structure introduced in Section 4.2 and 4.3, we can prove that for any MILP instance viewed as a sequence:

MILPnet can uniformly approximate MILP feasibility mapping, MILP optimal-solution mapping, and MILP optimal objective value mapping.

The following theorems formally establish MILPnet's approximation capabilities (see Appendix G for detailed proofs and corollary on infinite set):

Theorem 2. *Let $D \subset H^{MILP}$ be a finite dataset. For any $\epsilon > 0$, there exists a neural network $F_{HYA} \in \mathcal{F}^{MILPnet}_{HYA}$ such that:*

$$P\left(\mathbb{I}_{F_{HYA}(x)>\frac{1}{2}} \neq \Phi_{feas}(x)\right) < \epsilon, \quad \forall x \in D, \tag{9}$$

Theorem 3. *Let $D \subset H^{MILP}$ be a finite dataset. For any $\epsilon, \delta > 0$, there exist two neural networks $F_{HYA,1}, F_{HYA,2} \in \mathcal{F}^{MILPnet}_{HYA}$ such that for classifying whether the objective value is finite:*

$$P\left(\mathbb{I}_{F_{HYA,1}(x)>\frac{1}{2}} \neq \mathbb{I}_{\Phi_{obj}(x)\in\mathbb{R}}\right) < \epsilon, \quad \forall x \in D \tag{10}$$

where $\mathbb{I}_{\Phi_{obj}(x)\in\mathbb{R}}$ is an indicator function that determines whether the objective value is finite. And for the regression problem of predicting the objective value:

$$P\left(|F_{HYA,2}(x) - \Phi_{obj}(x)| > \delta\right) < \epsilon, \quad \forall x \in D \cap \Phi^{-1}_{obj}(\mathbb{R}) \tag{11}$$

Theorem 4. *Let $D \subset \Phi^{-1}_{obj}(\mathbb{R}) \subset H^{MILP}$ be a finite dataset. For any $\epsilon, \delta > 0$, there exists a Hybrid attention based network $F_{HYA,V} \in \mathcal{F}^{MILPnet}_{HYA,V}$ such that:*

$$P\left(\|F_{HYA,V}(x) - \Phi_{solu}(x)\| > \delta\right) < \epsilon, \quad \forall x \in D, \tag{12}$$

To train any MILPnet F_ϕ to approximate these mappings, we minimize the error between MILPnet and the feature mapping as the loss function $\mathcal{L}(\phi) = E[\|\mathbf{y} - F_\phi(x)\|_2]$, where $\mathbf{y}$ is ground truth.

6 Experiment

We conducted comprehensive experiments to evaluate the effectiveness, efficiency, and generalizability of MILPnet to answer:**RQ1:** How effectively does MILPnet represent and generalize on Foldable MILP instances? **RQ2:** How does MILPnet perform on real-world MILP instances? **RQ3:** How do MILPnet's architectural components impact performance?

Table 1: Generalization results for feasibility mapping on FOLD(20,*) and FOLD(50,*), with 10,000 foldable instances per setting and pre-training times of 3 and 10 minutes. Full results are provided in Appendix B.5.

Method	Type	FOLD(20,6)			FOLD(20,16)			FOLD(50,20)			FOLD(50,30)		
		MSE	ErrorN	Params	MSE	ErrorN	Params	MSE	ErrorN	Params	MSE	ErrorN	Params
SCIP	Exact	——	0	——	——	0	——	——	0	——	——	0	——
GCN	Graph	0.3073	5000	1.21M	0.3073	5000	1.21M	0.3073	5000	1.21M	0.3073	5000	1.21M
GIN	Graph	0.4200	5000	1.63M	0.4209	5000	1.63M	0.4200	5000	1.63M	0.4204	5000	1.63M
SAGE	Graph	0.4642	5000	0.66M	0.4999	5000	0.66M	0.4714	5000	0.66M	0.4586	5000	0.66M
PGN	Graph	0.2508	5000	1.64M	0.2523	5000	1.64M	0.2511	5000	1.64M	0.2511	5000	1.64M
GraphGPS	Graph	0.2500	5000	0.66M	0.2500	5000	0.66M	0.2500	5000	0.66M	0.2500	5000	0.66M
GCN^{rf}	Rf Graph	0.2498	5000	1.21M	0.2500	5000	1.21M	0.2476	4334	1.21M	0.5223	5000	1.21M
GIN^{rf}	Rf Graph	0.2500	5000	1.63M	0.2501	5000	1.63M	0.2500	5000	1.63M	0.4204	5000	1.63M
SAGE^{rf}	Rf Graph	0.2499	5009	0.66M	0.2499	4995	0.66M	0.2500	4997	0.66M	0.2500	5002	0.66M
PGN^{rf}	Rf Graph	0.2582	5000	1.64M	0.2560	5000	1.64M	0.2502	5000	1.64M	0.2502	5000	1.64M
GraphGPS^{rf}	Rf Graph	0.2510	5000	0.66M	0.2510	5000	0.66M	0.2500	5000	0.66M	0.2502	5000	0.66M
MILPnet	Ours (Seq)	**0.0005**	**0**	**0.56M**	**0.0004**	**0**	**0.56M**	**0.0005**	**0**	**0.60M**	**0.0023**	**12**	**0.60M**

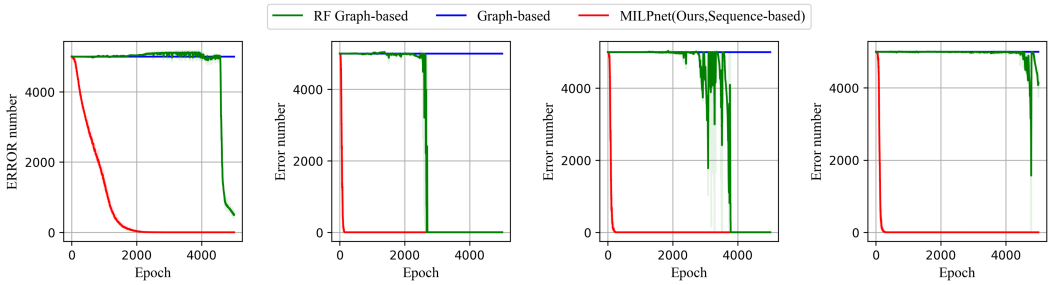

(a) FOLD(20,6) (b) FOLD(20,16) (c) FOLD(50,20) (d) FOLD(50,30)

Figure 3: Representation Dynamics on feasibility for FOLD20 and FOLD50. Full results are in Figure 9 in Appendix.

6.1 Experiment Setup

Datasets. We evaluate MILPnet on two categories of datasets: (1) *Synthetic Foldable MILP Instances (FOLD(n, m))*: Following (Chen et al., 2023b), we generate Foldable MILP instances where n and m are the number of variables and constraints, respectively. (2) *Real-World MILP Benchmarks*: We select four common MILP benchmarks: IP (Item Placement) from ML4CO competition dataset (Gasse et al., 2022), SC (Set Covering) (Feige, 1998; Chvátal, 1979), CA (Capacitated Assignment) (Bandyapadhyay et al., 2017), and FC (Facility Location) (Charikar et al., 1999). They are all Unfoldable MILP instances. More details on the datasets are provided in Appendix K.3 and Appendix K.5.

Baselines. We compare MILPnet against several representative graph-based learning models, including GCN (Chen et al., 2023b),GIN (Xu et al., 2019),SAGE (Wu et al., 2021),PGN (Cappart et al., 2022),GraphGPS (Wang et al., 2023b). Each baseline has an augmented variation with random features (RF), indicated by a superscript $*^{rf}$, specifically designed to overcome WL-test limitations in feasibility prediction. Appendix K.1 provides more details on the baselines.

Metrics. We use *MSE* (Mean Squared Error) and *ErrorN* (number of incorrect predictions)(Chen et al., 2023b), *Params* (number of model parameters) to evaluate performance. Lower is better.

6.2 Performance on Foldable MILP Instances

Representation Effectiveness. We evaluate *MILPnet* on Foldable MILP instances with increasing complexity: FOLD(20,6), FOLD(20,16), FOLD(50,20), and FOLD(50,30). Figure 3 shows that *MILPnet* converges rapidly to near-zero *ErrorN* while standard graph-based models fail to improve beyond their initial performance. Models with random feature augmentation show moderate improvements on simpler instances but struggle to converge on more complex cases such as FOLD(50,30). Similar trends are observed in MSE (more details in Appendix B.4). These results confirm that *MILP-*

Table 2: Generalization experiments for *End-to-End* optimal solution predict 1-hour of pre-train.

Method	Type	FOLD(20,6)		FOLD(20,16)	
		MSE	Params	MSE	Params
GCN	Graph	0.0751	1.17M	0.2000	1.17M
GIN	Graph	0.0753	1.59M	0.2000	1.59M
SAGE	Graph	0.0750	0.60M	0.2000	0.60M
PGN	Graph	70.1485	1.64M	20.5955	1.64M
GraphGPS	Graph	0.0863	0.60M	4.0395	0.60M
MILPnet(Ours)	Sequence	**0.0473**	**0.56M**	**0.1964**	**0.56M**
Method	Type	**FOLD(50,20)**		**FOLD(50,30)**	
		MSE	Params	MSE	Params
GCN	Graph	**0.1000**	1.17M	0.1509	1.17M
GIN	Graph	0.1000	1.59M	0.1501	1.59M
SAGE	Graph	0.1000	0.86M	0.1500	0.86M
PGN	Graph	55.8530	1.64M	36.5160	1.64M
GraphGPS	Graph	0.1020	0.67M	0.1551	0.67M
MILPnet(Ours)	Sequence	0.1158	**0.62M**	0.1654	**0.63M**

Table 3: Generalization experiments for *End-to-End* optimal objective value prediction

Method	Type	FOLD(20,6)		FOLD(20,16)	
		MSE	Params	MSE	Params
GCN	Graph	1.776e-10	0.88M	3.928e-10	0.58M
GIN	Graph	6.489e-10	0.12M	6.489e-10	0.16M
SAGE	Graph	2.235e-9	0.66M	6.742e-10	0.60M
PGN	Graph	1.958e-10	2.91M	5.4934e-10	2.91M
GraphGPS	Graph	3.769e-6	0.92M	1.365e-05	0.92M
MILPnet(Ours)	Sequence	**1.309e-10**	**0.56M**	**2.828e-10**	**0.56M**
Method	Type	**FOLD(50,20)**		**FOLD(50,30)**	
		MSE	Params	MSE	Params
GCN	Graph	3.333e-10	0.96M	5.8012e-10	0.96M
GIN	Graph	2.629e-10	1.30M	3.458e-10	1.47M
SAGE	Graph	1.219e-8	0.66M	7.555e-9	0.92M
PGN	Graph	3.935e-10	2.91M	3.762e-9	2.30M
GraphGPS	Graph	2.531e-7	0.92M	3.442e-6	0.92M
MILPnet(Ours)	Sequence	**9.458e-12**	**0.60M**	**3.007e-10**	**0.60M**

Table 4: Generalization results for feasibility prediction on larger Foldable instances FOLD(200,20), FOLD(300,40), and FOLD(500,60), each with 10,000 instances and 1 hour of pre-training.

Method	Type	FOLD(200,20)			FOLD(300,40)			FOLD(500,60)		
		MSE	ErrorN	Params	MSE	ErrorN	Params	MSE	ErrorN	Params
SCIP	Exact	——	0	——	——	0	——	——	0	——
GCN	Graph	0.2676	5000	0.03M	0.3073	5000	0.08M	0.2500	4999	0.14M
GIN	Graph	0.2573	5000	0.04M	0.3099	5000	0.10M	0.2500	5000	0.21M
SAGE	Graph	0.2814	5000	0.03M	0.3951	5000	0.05M	0.2500	5000	0.12M
PGN	Graph	0.2508	5000	0.08M	0.2523	5000	0.14M	0.2523	5000	0.29M
GraphGPS	Graph	0.2500	5000	0.03M	0.2500	5000	0.59M	0.2501	5000	0.92M
GCN^{rf}	Rf Graph	0.2497	4835	0.03M	0.2500	5000	0.80M	0.2611	4999	0.14M
GIN^{rf}	Rf Graph	0.2500	4998	0.04M	0.2500	5012	0.10M	0.2501	5003	0.21M
$SAGE^{rf}$	Rf Graph	0.2500	5011	0.03M	0.2500	4998	0.05M	0.2500	4981	0.12M
PGN^{rf}	Rf Graph	0.2544	5000	0.08M	0.2500	5000	0.14M	0.2506	5000	0.29M
$GraphGPS^{rf}$	Rf Graph	0.2502	5000	0.03M	0.2510	5000	0.05M	0.2506	5000	0.92M
MILPnet	Seq (Ours)	**0.0155**	**191**	**0.02M**	**0.0521**	**560**	**0.04M**	**0.1832**	**2453**	**0.11M**

net effectively captures the geometric and combinatorial structure of MILPs, providing empirical support for the theoretical guarantees in Theorems 2–4.

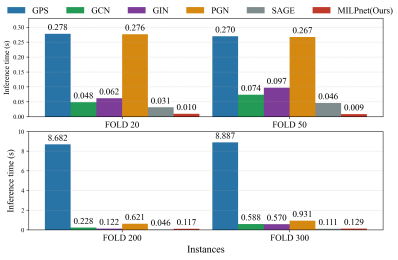

Figure 4: Inference time comparisons

Generalization Abilities. We evaluate *MILPnet* on both small (FOLD(20,*), FOLD(50,*)) and large (FOLD(200,20), FOLD(300,40), and FOLD(500,60)) Foldable MILP instances under equal pre-training time, focusing on three *End-to-End* prediction tasks: feasibility, optimal solution, and optimal objective value. In feasibility prediction (Tables 1 and 4), *MILPnet* improves MSE by 1–3 orders of magnitude and reduces *ErrorN* by 90% or more in most cases. For optimal solution and value prediction (Tables 2 and 3), *MILPnet* significantly exceeds baselines while using substantially fewer parameters.

Efficiency Analysis and Sparse Variant. Figure 4 shows that *MILPnet* consistently achieves the fastest inference time across both small and large Foldable MILPs. GPU memory usage (Appendix Figure 13) remains moderate (< 4GB on FOLD300), making it suitable for deployment on a wide range of hardware. We also provide a sparse (stride) MILPnet variant that reduces the time complexity to $\frac{1}{s}$ of the original, with *FOLD*200 faster inference results shown in Table 14 and details in the AppendixJ,indicates its potential computational scalability.

Overall Model Comparison. We summarize performance across key metrics, including generalization, parameter count, inference time, GPU memory, and *ErrorN*, using radar charts with performance ranks(Figures 1 for FOLD50 and Appendix Figure 14 for FOLD300). In both cases, *MILPnet* consistently forms the outermost polygon, indicating superior performance in accuracy, efficiency, and resource usage compared to graph-based baselines.

Table 5: *Predict + Search* performance of MILPnet on four benchmarks. "Rand" denotes randomly generated initial solutions. "gap" is computed as gap $= (\hat{y} - y^*) \,/\, (|y^*| + 10^{-9})$, where y^* is the exact optimal value by SCIP."PT" means the predicting optimal candidate solution. "ST" is total solving time including search. Full Comparisons with advanced methods are in Appendix C.1.

Method	Type	IP			SC			CA			FC		
		gap(↓)	PT(s) (↓)	ST(s) (↓)	gap(↓)	PT(s) (↓)	ST(s) (↓)	gap(↓)	PT(s) (↓)	ST(s) (↓)	gap(↓)	PT(s) (↓)	ST(s) (↓)
Rand	Random	36.5397	——	0.1240	1.7166	——	2.0173	2.8057	——	6.7830	1.4939	——	1.7786
GCN	Graph	0.0389	0.2443	0.3774	1.1461	0.2391	0.8386	0.9890	0.2278	3.2328	0.4257	0.2518	1.4875
MILPnet	Seq(Ours)	**0.0234**	**0.0625**	**0.1864**	**0.3483**	**0.0137**	**0.6915**	**0.7651**	**0.0139**	**3.2300**	**0.3503**	**0.0177**	**1.3773**

Table 6: Performance impact of MILPnet's architectural components

(a) Ablation results on the impact of HYA and MSA

Method	FOLD(20,6)		FOLD(50,20)		FOLD(100,20)	
	MSE	ErrorN	MSE	ErrorN	MSE	ErrorN
MILPnet (ours)	**0.0001**	**0**	**0.0001**	**0**	**0.0074**	**6**
w/o HYA	0.2503	5036	0.2501	4999	0.2501	4987
w/o MSA	0.2500	5051	0.2500	5008	0.2500	4995

(b) Impact of $\eta_{\max}$ ("/n" means $\eta_{\max} = n$)

Method	FOLD(20,6)		FOLD(50,30)		FOLD(100,20)	
	MSE	ErrorN	MSE	ErrorN	MSE	ErrorN
MILPnet /2	**0.0005**	**0**	**0.0477**	**235**	0.0558	318
MILPnet /3	0.0006	0	0.0481	259	**0.0471**	**272**
MILPnet /4	0.0026	0	0.0841	764	0.0774	727

6.3 Performance on Real-World MILP Instances

While our focus is on sequence-based representation, we further demonstrate the utility of *MILPnet* in solving real-world MILP problems. We adopt a *predict + search* approach, where the model is trained to predict an optimal solution, which is then refined via a lightweight local heuristic. Table 5 compares MILPnet with graph-based baselines and a random search baseline. *MILPnet* consistently achieves the smallest optimality gap to the exact solver, and the lowest overall solving time. These results demonstrate the model's strong representation quality and practical solving effectiveness.

6.4 Impact of Architectural Components

Ablation Study on Hybrid and Multi-scale Attention. To evaluate the contribution of MILPnet's attention design, we compare the removal of the Hybrid Attention (HYA) and Multi-Scale Attention (MSA) components. Table 6a shows that removing either component significantly degrades feasibility prediction accuracy. In particular, models without MSA struggle to capture local structure, while disabling HYA weakens global context integration. These results confirm that both components are essential to MILPnet's representation effectiveness.

Table 7: Permutation invariance Experiments. "Or *" represents randomly permutated constraint order in the MILP-sequence."Original *"represents the original order.

Order	Method + Arch	FOLD(50,20)		FOLD(50,30)	
		MSE	ErrorN	MSE	ErrorN
GCN (Original)	GNN + Graph	0.4719	5000	0.4719	5000
Original	MILPnet + Seq	0.0005	0	0.0022	0
Or 1	MILPnet + Seq	0.0006	0	0.0021	0
Or 2	MILPnet + Seq	0.0001	0	0.0014	0
Or 3	MILPnet + Seq	0.0004	0	0.0021	9

Ablation study on multi-scale attention blocks We conduct an ablation study on the depth of the multi-scale attention module by varying the number of blocks from 1 to 3. The results, which visualize and summarize its representational and generalization capabilities, are provided in Figure 8 in the Appendix B and Table 8. A key finding is that deeper multi-scale attention modules offer a significant improvement in convergence speed and representation at no cost to generalization ability.

Table 8: Ablation study on the number of multi-scale attention blocks (L).

Number of blocks	Method + Arch	FOLD(20,16)		FOLD(50,20)	
		MSE	ErrorN	MSE	ErrorN
GCN (Original)	GNN + Graph	0.3070	5000	0.4719	5000
L=1	MILPnet + Seq	0.0006	0	0.0003	0
L=2	MILPnet + Seq	0.0001	0	0.0001	0
L=3	MILPnet + Seq	0.0004	0	0.0001	0

Impact of the Maximum Window Size As shown in Tables 6b (pre-train 5mins) and Appendix Fig 7, the maximum window size $\eta_{\max}$ influences the trade-off between convergence speed and representational capacity. Smaller windows accelerate convergence on simpler instances like FOLD(20,), while large windows slow training and degrade performance on complex cases such as FOLD(100,20). These results indicate that $\eta_{\max}$ requires careful tuning and does not follow a monotonic pattern.

Permutation Sensitivity of MILP-sequence. Randomly shuffling the constraint and variable order in FOLD520 and FOLD50 keeps MILPnet's MSE within the same magnitude (Table 7,11 in Appendix B) and well below that of other models (typical MSE $\approx$ 0.x, error $\approx$ 5000). These results demonstrate that ours MILP-sequence construction preserves invariance under both constraint and variable permutations.

6.5 MILPNET SOLVING EFFICIENCY ANALYSIS

We analyze the solving efficiency of MILPnet across two dimensions: **(i)** Large-scale public MILP benchmarks (with 1000+ variables, details in the Appendix) to evaluate each framework component; **(ii)** Heterogeneous generalization and scalability on four very large real-world benchmarks (with 10000+ variables). To quantify solution quality in details, we integrate both MILPNet and graph-based baselines as pre-solving heuristics using Neural Diving (Paulus & Krause, 2023b) to obtain compact sub-problems within a branch-and-bound framework for **(i)**.

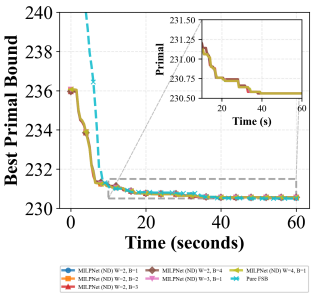

Figure 5: Neural pre solving by MILPnet for SC(1000,500) for 6 settings.

Impact of Window Size $\eta_{\max}$ and Attention Depth L We evaluate the impact of maximum window size $\eta_{\max}$ and attention depth L on two large MILP benchmarks. Table 9 and Figure 5 show that performance is relatively insensitive to these hyperparameters, with consistent improvements (*Nodes,Time,Dual Gap,Obj*) over graph-based methods and Strong Branching across all configurations.

Table 9: *Branch and Bound* performance of MILPnet (Neural Diving based pre-solving heuristic: H.Seq.) on 1000+ variable benchmarks for 50 instances within 60s solving limit.

Method	Type	SC(1000,500)				CA(1000,500)			
		Obj.(↓)	Node(↓)	Time (↓)	Dual Gap	Obj.(↑)	Node(↓)	Time (↓)	Dual Gap
SB	Exact	**230.5** ± 28.3	39.0 ± 41.2	19.1 ± 15.0	0.21± 1.23(%)	146.0 ± 26.6	1.0 ± 0.0	3.4 ± 1.0	0.00±0.00(%)
Rand	Random	235.9 ± 30.5	40.1 ± 45.3	20.0 ± 14.9	0.21± 1.23(%)	146.0 ± 26.6	1.0 ± 0.0	3.4 ± 1.0	0.00±0.00(%)
GIN	H. Graph	230.5 ± 28.3	38.8 ± 40.0	18.6 ± 15.4	0.21± 1.23(%)	146.0 ± 26.6	1.0 ± 0.0	1.8 ± 0.2	0.00±0.00(%)
GraphGPS	H. Graph	230.5 ± 28.3	38.9 ± 44.8	17.9 ± 15.1	0.21± 1.23(%)	146.0 ± 26.6	1.0 ± 0.0	1.8 ± 0.2	0.00±0.00(%)
MILPnet/2	H. Seq. L=1	230.5 ± 28.3	37.7 ± 39.8	16.5 ± 15.5	0.21± 1.23(%)	146.0 ± 26.6	1.0 ± 0.0	1.7 ± 0.2	0.00±0.00(%)
MILPnet/2	H. Seq. L=2	230.5 ± 28.3	**37.7** ± 39.8	16.5 ± 15.6	0.21± 1.23(%)	**146.0** ± 26.6	1.0 ± 0.0	**1.5** ± 0.2	0.00±0.00(%)
MILPnet/2	H. Seq. L=3	230.5 ± 28.3	38.5 ± 41.0	**16.2** ± 15.4	0.17± 1.21(%)	146.0 ± 26.6	1.0 ± 0.0	1.5 ± 0.2	0.00±0.00(%)
MILPnet/2	H. Seq. L=4	230.5 ± 28.3	38.3 ± 42.0	16.3 ± 15.5	**0.17**± 1.21(%)	146.0 ± 26.6	1.0 ± 0.0	1.5 ± 0.2	**0.00**±0.00(%)
MILPnet/3	H. Seq. L=1	230.5 ± 28.3	37.7 ± 39.9	16.5 ± 15.5	0.21± 1.23(%)	146.0 ± 26.6	1.0 ± 0.0	1.7 ± 0.2	0.00±0.00(%)
MILPnet/4	H. Seq. L=1	230.5 ± 28.3	37.7 ± 39.8	16.5 ± 15.5	0.21± 1.23(%)	146.0 ± 26.6	1.0 ± 0.0	1.7 ± 0.2	0.00±0.00(%)

Heterogeneous solving generalization To assess heterogeneous generalization capability, we integrate MILPnet as a novel representation framework that replaces graph-based representations in advanced ML solvers such as ConPAS. Trained on the SC dataset, MILPnet is directly transferred to solve very large MILP instances from open-source benchmarks (Gleixner et al., 2021). The results, including primal bound iterations (Fig.12 in Appendix) and solving efficiency (Table 10), demonstrate that MILPnet generalizes stably and scalably across heterogeneous, large-scale benchmarks, achieving consistent performance improvements in all tested cases.Details are in Appendix C.2.

Table 10: Heterogeneous generalization on *very-large benchmarks* (Gleixner et al., 2021) within 1500s.

Method	**30n20b8** 18.4K		**blp-ic98** 13.6K		**blp-ar98** 16.0K	
	Time	Obj	Time	Obj	Time	Obj
SCIP	163.96	302.00	1500.15	4620.13	1500.10	6215.35
ConPAS(GCN)	175.86	302.00	1500.00	4817.66	1500.01	6254.08
ConPAS(MILPnet)	**94.64**	**302.00**	**1500.00**	**4588.51**	**1500.01**	**6220.57**

7 CONCLUSION

We propose *MILPnet*, a novel multi-scale hybrid framework for representing MILP problems through sequence modeling, rather than conventional graph methods. We prove that this architecture can approximate essential MILP mappings for arbitrary instances. Empirical evaluation confirms that *MILPnet* outperforms graph-based methods in terms of efficiency and performance, while addressing the Foldable MILPs where graph-based approaches fail.

Reproducibility statement

Our work is fully reproducible. Source code is available at https://anonymous.4open.science/r/MILPnet-2BD1/. All datasets, experiments, and architecture hyperparameters used in our experiments are documented in the Appendix K and Appendix B.

References

Charalambos D Aliprantis and Kim C Border. *Infinite Dimensional Analysis: A Hitchhiker's Guide*. Springer, Berlin, 3rd edition, 2006.

Sayan Bandyapadhyay, Santanu Bhowmick, Tanmay Inamdar, and Kasturi Varadarajan. Capacitated covering problems in geometric spaces, 2017. URL https://arxiv.org/abs/1707.05170.

Yoshua Bengio, Andrea Lodi, and Antoine Prouvost. Machine learning for combinatorial optimization: a methodological tour d'horizon. *CoRR*, abs/1811.06128, 2018. URL http://arxiv.org/abs/1811.06128.

Quentin Cappart, Didier Chételat, Elias Khalil, Andrea Lodi, Christopher Morris, and Petar Veličković. Combinatorial optimization and reasoning with graph neural networks, 2022. URL https://arxiv.org/abs/2102.09544.

Moses Charikar, Sudipto Guha, Éva Tardos, and David B. Shmoys. A constant-factor approximation algorithm for the k-median problem (extended abstract). In *Proceedings of the Thirty-First Annual ACM Symposium on Theory of Computing*, STOC '99, pp. 1–10, New York, NY, USA, 1999. Association for Computing Machinery. ISBN 1581130678. doi: 10.1145/301250.301257. URL https://doi.org/10.1145/301250.301257.

Hao Chen, Kai-Chieh Hsu, Walker J. Turner, Po-Hsuan Wei, Keren Zhu, David Z. Pan, and Haoxing Ren. Reinforcement learning guided detailed routing for custom circuits. In *Proceedings of the 2023 International Symposium on Physical Design*, ISPD '23, pp. 26–34, New York, NY, USA, 2023a. Association for Computing Machinery. ISBN 9781450399784. doi: 10.1145/3569052.3571874.

Lin Chen, Yiran Liu, Zehan Qi, Zhaoyuan Wu, and Yang Yu. Constraint-adaptive reinforcement learning for large-scale power system planning. November 2024. doi: 10.36227/techrxiv.173161402.22049085/v1.

Ziang Chen, Jialin Liu, Xinshang Wang, Jianfeng Lu, and Wotao Yin. On representing mixed-integer linear programs by graph neural networks, 2023b. URL https://arxiv.org/abs/2210.10759.

Antonia Chmiela, Elias B. Khalil, Ambros Gleixner, Andrea Lodi, and Sebastian Pokutta. Learning to schedule heuristics in branch-and-bound, 2021. URL https://arxiv.org/abs/2103.10294.

V. Chvátal. A greedy heuristic for the set-covering problem. *Mathematics of Operations Research*, 4 (3):233–235, 1979. doi: 10.2307/3689577.

Michele Conforti, Gérard Cornuéjols, and Giacomo Zambelli. *Polyhedral Approaches to Mixed Integer Linear Programming*, pp. 343–385. Springer Berlin Heidelberg, Berlin, Heidelberg, 2010. ISBN 978-3-540-68279-0. doi: 10.1007/978-3-540-68279-0_11. URL https://doi.org/10.1007/978-3-540-68279-0_11.

L. E Dubins and L. J Savage. How to gamble if you must. 2014.

Uriel Feige. A threshold of ln n for approximating set cover. *J. ACM*, 45(4):634–652, July 1998. ISSN 0004-5411. doi: 10.1145/285055.285059. URL https://doi.org/10.1145/285055.285059.

Maxime Gasse, Didier Chételat, Nicola Ferroni, Laurent Charlin, and Andrea Lodi. Exact combinatorial optimization with graph convolutional neural networks. *CoRR*, abs/1906.01629, 2019. URL http://arxiv.org/abs/1906.01629.

Maxime Gasse, Quentin Cappart, Jonas Charfreitag, Laurent Charlin, Didier Chételat, Antonia Chmiela, Justin Dumouchelle, Ambros Gleixner, Aleksandr M. Kazachkov, Elias Khalil, Pawel Lichocki, Andrea Lodi, Miles Lubin, Chris J. Maddison, Christopher Morris, Dimitri J. Papageorgiou, Augustin Parjadis, Sebastian Pokutta, Antoine Prouvost, Lara Scavuzzo, Giulia Zarpellon, Linxin Yang, Sha Lai, Akang Wang, Xiaodong Luo, Xiang Zhou, Haohan Huang, Shengcheng Shao, Yuanming Zhu, Dong Zhang, Tao Quan, Zixuan Cao, Yang Xu, Zhewei Huang, Shuchang Zhou, Chen Binbin, He Minggui, Hao Hao, Zhang Zhiyu, An Zhiwu, and Mao Kun. The machine learning for combinatorial optimization competition (ml4co): Results and insights, 2022. URL https://arxiv.org/abs/2203.02433.

Zijie Geng, Xijun Li, Jie Wang, Xiao Li, Yongdong Zhang, and Feng Wu. A deep instance generative framework for milp solvers under limited data availability, 2024. URL https://arxiv.org/abs/2310.02807.

Ambros Gleixner, Gregor Hendel, Gerald Gamrath, Tobias Achterberg, Michael Bastubbe, Timo Berthold, Philipp M. Christophel, Kati Jarck, Thorsten Koch, Jeff Linderoth, Marco Lübbecke, Hans D. Mittelmann, Derya Ozyurt, Ted K. Ralphs, Domenico Salvagnin, and Yuji Shinano. MIPLIB 2017: Data-Driven Compilation of the 6th Mixed-Integer Programming Library. *Mathematical Programming Computation*, 2021. doi: 10.1007/s12532-020-00194-3. URL https://doi.org/10.1007/s12532-020-00194-3.

Michael Goldman and Dario Trevisan. Optimal transport methods for combinatorial optimization over two random point sets, 2023.

Ralph E. Gomory. An algorithm for integer solutions to linear programs. 1958.

Prateek Gupta, Maxime Gasse, Elias B. Khalil, M. Pawan Kumar, Andrea Lodi, and Yoshua Bengio. Hybrid models for learning to branch. *CoRR*, abs/2006.15212, 2020. URL https://arxiv.org/abs/2006.15212.

Qingyu Han, Linxin Yang, Qian Chen, Xiang Zhou, Dong Zhang, Akang Wang, Ruoyu Sun, and Xiaodong Luo. A gnn-guided predict-and-search framework for mixed-integer linear programming, 2023. URL https://arxiv.org/abs/2302.05636.

He He, Hal Daume III, and Jason M Eisner. Learning to search in branch and bound algorithms. In Z. Ghahramani, M. Welling, C. Cortes, N. Lawrence, and K.Q. Weinberger (eds.), *Advances in Neural Information Processing Systems*, volume 27. Curran Associates, Inc., 2014.

Taoan Huang, Aaron Ferber, Yuandong Tian, Bistra Dilkina, and Benoit Steiner. Searching large neighborhoods for integer linear programs with contrastive learning, 2023. URL https://arxiv.org/abs/2302.01578.

Joey Huchette and Juan Pablo Vielma. A geometric way to build strong mixed-integer programming formulations, 2019. URL https://arxiv.org/abs/1811.10409.

Ailsa H. Land and Alison G. Doig. An automatic method of solving discrete programming problems. *Econometrica*, 28:497, 1960.

He Ma, Wenlian Lu, and Jianfeng Feng. Efficient combinatorial optimization via heat diffusion. *ArXiv*, abs/2403.08757, 2024. URL https://api.semanticscholar.org/CorpusID:268379750.

Zoubir Mammeri. Reinforcement learning based routing in networks: Review and classification of approaches. *IEEE Access*, 7:55916–55950, 2019. doi: 10.1109/ACCESS.2019.2913776.

J. V. Neumann. On a certain topology for rings of operators. *Annals of Mathematics*, 37(1):111–115, 1936.

Max B. Paulus and Andreas Krause. Learning to dive in branch and bound, 2023a. URL https://arxiv.org/abs/2301.09943.

Max B. Paulus and Andreas Krause. Learning to dive in branch and bound, 2023b. URL https://arxiv.org/abs/2301.09943.

Sebastian Sanokowski, Sepp Hochreiter, and Sebastian Lehner. A diffusion model framework for unsupervised neural combinatorial optimization, 2024. URL https://arxiv.org/abs/2406.01661.

Zhiqing Sun and Yiming Yang. Difusco: Graph-based diffusion solvers for combinatorial optimization, 2023. URL https://arxiv.org/abs/2302.08224.

Wei tian Wu and Xin min Yang. The hybridization of branch and bound with metaheuristics for nonconvex multiobjective optimization, 2022.

Jie Wang, Zhihai Wang, Xijun Li, Yufei Kuang, Zhihao Shi, Fangzhou Zhu, Mingxuan Yuan, Jia Zeng, Yongdong Zhang, and Feng Wu. Learning to cut via hierarchical sequence/set model for efficient mixed-integer programming, 2024.

Shaohua Wang, Junyuan Zhou, Haojian Liang, Zhenbo Wang, Cheng Su, and Xiao Li. A new approach for solving location routing problems with deep reinforcement learning of emergency medical facility. In *Proceedings of the 8th ACM SIGSPATIAL International Workshop on Security Response Using GIS*, EM-GIS '23, pp. 50–53, New York, NY, USA, 2023a. Association for Computing Machinery. ISBN 9798400703461. doi: 10.1145/3615884.3629429. URL https://doi.org/10.1145/3615884.3629429.

Tianze Wang, Amir H. Payberah, and Vladimir Vlassov. Graph representation learning with graph transformers in neural combinatorial optimization. In *2023 International Conference on Machine Learning and Applications (ICMLA)*, pp. 488–495, 2023b. doi: 10.1109/ICMLA58977.2023.00074.

Zonghan Wu, Shirui Pan, Fengwen Chen, Guodong Long, Chengqi Zhang, and Philip S. Yu. A comprehensive survey on graph neural networks. *IEEE Transactions on Neural Networks and Learning Systems*, 32(1):4–24, January 2021. ISSN 2162-2388. doi: 10.1109/tnnls.2020.2978386. URL http://dx.doi.org/10.1109/TNNLS.2020.2978386.

Keyulu Xu, Weihua Hu, Jure Leskovec, and Stefanie Jegelka. How powerful are graph neural networks?, 2019. URL https://arxiv.org/abs/1810.00826.

Huigen Ye, Hua Xu, Hongyan Wang, Chengming Wang, and Yu Jiang. Gnn & gbdt-guided fast optimizing framework for large-scale integer programming. In Andreas Krause, Emma Brunskill, Kyunghyun Cho, Barbara Engelhardt, Sivan Sabato, and Jonathan Scarlett (eds.), *Proceedings of the 40th International Conference on Machine Learning*, volume 202 of *Proceedings of Machine Learning Research*, pp. 39864–39878. PMLR, 23–29 Jul 2023. URL https://proceedings.mlr.press/v202/ye23e.html.

Gilad Yehudai, Ethan Fetaya, Eli Meirom, Gal Chechik, and Haggai Maron. From local structures to size generalization in graph neural networks, 2021. URL https://arxiv.org/abs/2010.08853.

Kexiong Yu, Hang Zhao, Yuhang Huang, Renjiao Yi, Kai Xu, and Chenyang Zhu. Disco: Efficient diffusion solver for large-scale combinatorial optimization problems, 2024. URL https://arxiv.org/abs/2406.19705.

Zidong Zhang, Dongxia Zhang, and Robert C. Qiu. Deep reinforcement learning for power system applications: An overview. *CSEE Journal of Power and Energy Systems*, 6(1):213–225, 2020. doi: 10.17775/CSEEJPES.2019.00920.

A Detailed Architecture for MILPnet

Figure 6 illustrates the detailed architecture of MILPnet, which connects a feed-forward network with the core Multi-scale based Hybrid Attention.

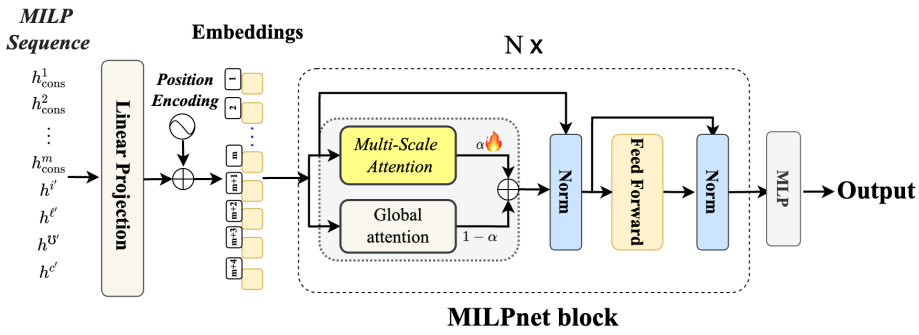

Figure 6: Detailed Architecture of *MILPnet*.

B Full Results on Maximum Window Size, Attention blocks, Representation, and Generalization

B.1 Ablation studies on the η_{max}

We conducted a study on the maximum sliding-window size and visualized the resulting representation curves in Figure 7.

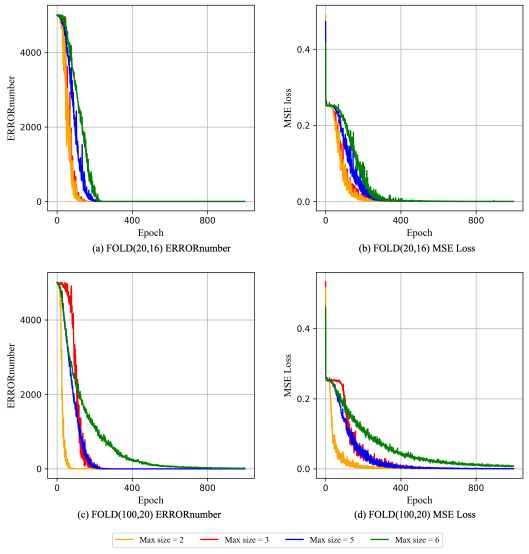

Figure 7: Performance of varied max window size of MILPnet on FOLD(20,16) and FOLD(100,20) for feasibility. We can observe that the maximum sliding window size affects the convergence speed of the feasibility mapping approximation. The window size does not follow a simple pattern, but rather requires balancing.

B.2 ABLATION STUDY ON THE NUMBER OF ATTENTION BLOCKS L

We conduct the ablation study on the number of attention blocks on FOLD(20) and FOLD(50).

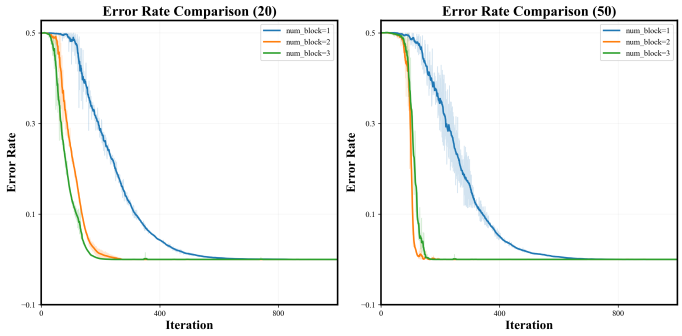

Figure 8: Performance of varied numbers of multi-scale attention blocks in MILPnet on FOLD(20,16) and FOLD(50,20) for feasibility with the same embedding size and same window size for blocks =1,2,3.

B.3 PERMUTATION SENSITIVITY ON VARIABLE ORDERS

Table 11: Experiments on variable permutation invariance. "V-Or *" represents randomly permutated variable order in the MILP-sequence."Original *"represents the original order.

Order	Method + Arch	**FOLD(20,16)**		**FOLD(50,20)**	
		MSE	ErrorN	MSE	ErrorN
GCN (Original)	GNN + Graph	0.3070	5000	0.4719	5000
Original	MILPnet + Seq	0.0003	0	0.0003	0
V-Or 1	MILPnet + Seq	0.0006	0	0.0001	5
V-Or 2	MILPnet + Seq	0.0003	0	0.0003	0
V-Or 3	MILPnet + Seq	0.0004	0	0.0005	3

B.4 REPRESENTATION EXPERIMENTS

We conducted representation experiments on the representation of feasible mapping, the optimal solution mapping, and the objective optimal value, for MILP instances. The embedding sizes used in our experiments were chosen from $\{32, 128, 216, 256, 512\}$. Figure 9 shows the representation results of feasible mapping, Figure 10 shows the results of optimal solution mapping, and Figure 15 shows the results of the objective optimal value mapping.

B.5 GENERALIZATION EXPERIMENTS RESULTS

We provide the full results on FOLD(20,) to FOLD(50,) in Table 9 following.

B.6 CROSS-SIZE ADAPTION

Our approach also enables *End to End Cross-Size* generalization from FOLD(n,m_1) to FOLD(n,m_2), which is quite difficult for Bipartite Graph-based MILP *End-to-End* representation methods(Yehudai et al., 2021). We directly transfer the network pre-trained on FOLD (50,20) on the feasibility mapping to FOLD (50,30). As shown by the heatmap, the pre-trained network also easily achieves good performance on FOLD (50,30), which demonstrates that our model can still perform inference directly when faced with changes in length, effectively transferring its prior knowledge. This verifies that our network can effectively extract features.

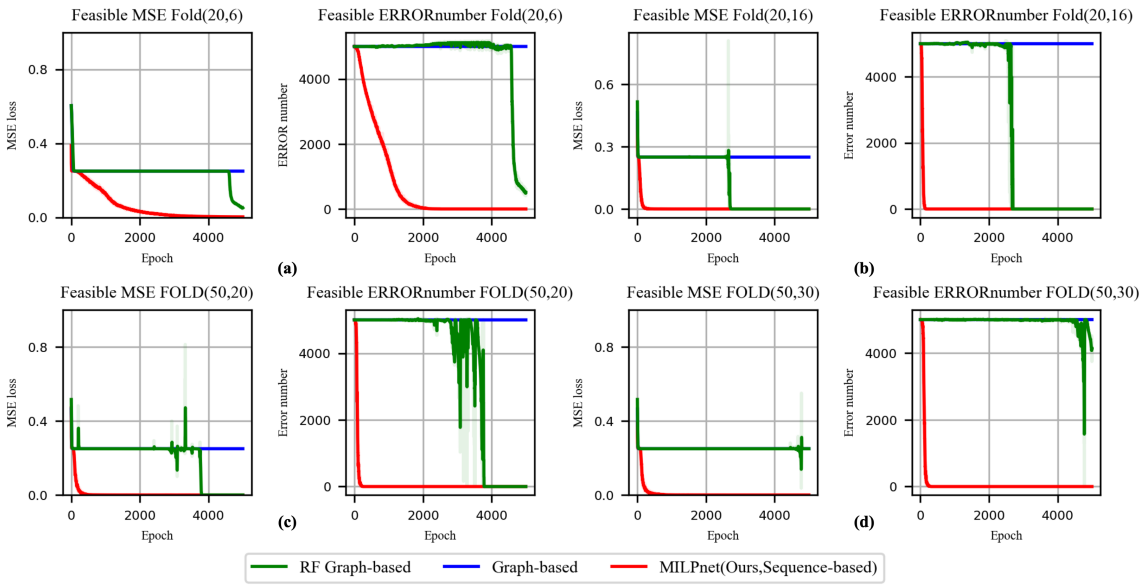

Figure 9: Representation experiments on feasibility for FOLD20 ((a) for FOLD(20,6), (b) for FOLD(20,16)) and FOLD50 ((c) for FOLD(50,20),(d) for FOLD(50,30)). **MILPnet** approximates the feasible mapping of Foldable MILP instances more efficiently.

Table 12: Generalization experiments for feasibility mapping on FOLD(20,*) to FOLD(50,*), with 10,000 foldable MILP instances from each.3M(20)/10M(50) means pre-train time for FOLD20 is 3mins, FOLD50 is 10mins;5M(20)/30M(50) means pre-train time for FOLD20 is 5mins, FOLD50 is 30mins.

Method	Type	FOLD(20,6)			FOLD(20,16)			FOLD(50,20)			FOLD(50,30)		
		MSE	ErrorN	Params	MSE	ErrorN	Params	MSE	ErrorN	Params	MSE	ErrorN	Params
SCIP	Exact	——	0	——	——	0	——	——	0	——	——	0	——
$GCN_{3M(20)/10M(50)}$	Graph	0.3073	5000	1.21M	0.3073	5000	1.21M	0.3073	5000	1.21M	0.3073	5000	1.21M
$GCN_{5M(20)/30M(50)}$	Graph	0.3073	5000	1.21M	0.3070	5000	1.21M	0.4719	5000	1.21M	0.4719	5000	1.21M
$GIN_{3M(20)/10M(50)}$	Graph	0.4200	5000	1.63M	0.4209	5000	1.63M	0.4200	5000	1.63M	0.4204	5000	1.63M
$GIN_{5M(20)/30M(50)}$	Graph	0.4199	5000	1.63M	0.2999	5000	1.63M	0.2939	5000	1.63M	0.4204	5000	1.63M
$SAGE_{3M(20)/10M(50)}$	Graph	0.4642	5000	0.66M	0.4999	5000	0.66M	0.4714	5000	0.66M	0.4586	5000	0.66M
$SAGE_{5M(20)/30M(50)}$	Graph	0.4642	5000	0.66M	0.4999	5000	0.66M	0.4714	5000	0.66M	0.4856	5000	0.66M
$PGN_{3M(20)/10M(50)}$	Graph	0.2508	5000	1.64M	0.2523	5000	1.64M	0.2511	5000	1.64M	0.2511	5000	1.64M
$PGN_{5M(20)/30M(50)}$	Graph	0.2511	5000	1.64M	0.2511	5000	1.64M	0.2512	5000	1.64M	0.2512	5000	1.64M
$GraphGPS_{3M(20)/10M(50)}$	Graph	0.2500	5000	0.66M	0.2500	5000	0.66M	0.2500	5000	0.66M	0.2500	5000	0.66M
$GraphGPS_{5M(20)/30M(50)}$	Graph	0.2500	5000	0.66M	0.2500	5000	0.66M	0.2500	5000	0.66M	0.2500	5000	0.66M
$GCN^{rf}_{5M(20)/30M(50)}$	Rf Graph	0.2498	5000	1.21M	0.2500	5000	1.21M	0.2476	4334	1.21M	0.5223	5000	1.21M
$GCN^{rf}_{5M(20)/30M(50)}$	Rf Graph	0.2126	2853	1.21M	0.2499	4921	1.21M	0.1177	0	1.21M	0.2402	0	1.21M
$GIN^{rf}_{3M(20)/10M(50)}$	Rf Graph	0.2500	5000	1.63M	0.2501	5000	1.63M	0.2500	5000	1.63M	0.4204	5000	1.63M
$GIN^{rf}_{5M(20)/30M(50)}$	Rf Graph	0.2499	4757	1.63M	0.2500	5000	1.63M	0.2500	5000	1.63M	0.2458	2603	1.63M
$SAGE^{rf}_{3M(20)/10M(50)}$	Rf Graph	0.2499	5009	0.66M	0.2499	4995	0.66M	0.2500	4997	0.66M	0.2500	5002	0.66M
$SAGE^{rf}_{5M(20)/30M(50)}$	Rf Graph	0.2499	5009	0.66M	0.2499	4995	0.66M	0.2500	4998	0.66M	0.2500	4999	0.66M
$PGN^{rf}_{3M(20)/10M(50)}$	Rf Graph	0.2582	5000	1.64M	0.2560	5000	1.64M	0.2502	5000	1.64M	0.2502	5000	1.64M
$PGN^{rf}_{5M(20)/30M(50)}$	Rf Graph	0.2507	5000	1.64M	0.2514	5000	1.64M	0.2512	5000	1.64M	0.2502	5000	1.64M
$GraphGPS^{rf}_{3M(20)/10M(50)}$	Rf Graph	0.2510	5000	0.66M	0.2510	5000	0.66M	0.2500	5000	0.66M	0.2502	5000	0.66M
$GraphGPS^{rf}_{5M(20)/30M(50)}$	Rf Graph	0.2510	5000	0.66M	0.2510	5000	0.66M	0.2500	5000	0.66M	0.2520	5000	0.66M
$MILPnet_{3M(20)/10M(50)}$	Ours (Seq)	0.0005	**0**	**0.56M**	0.0004	**0**	**0.56M**	0.0005	**0**	**0.60M**	**0.0023**	12	**0.60M**
$MILPnet_{5M(20)/30M(50)}$	Ours (Seq)	**0.0003**	**0**	**0.56M**	**8.53e-5**	**0**	**0.56M**	**0.0005**	**0**	**0.60M**	0.0082	**0**	**0.60M**

C MILPNET SOLVING EFFICIENCY RESULTS

C.1 ADDITIONAL EXPERIMENTS ON REAL-WORLD BENCHMARKS

This part, we use MILPnet and advanced graph-based network for predicting the near-optimal solution and refine by a local heuristic algorithm, the results are summarized in following Table 13. This result demonstrate that MILPnet consistently outperforms these advanced graph-based models in terms of solving efficiency and inference speed. This further validates the effectiveness of the sequence-based architecture and the representation advantage of MILP-sequence. For SC and CA with 1000

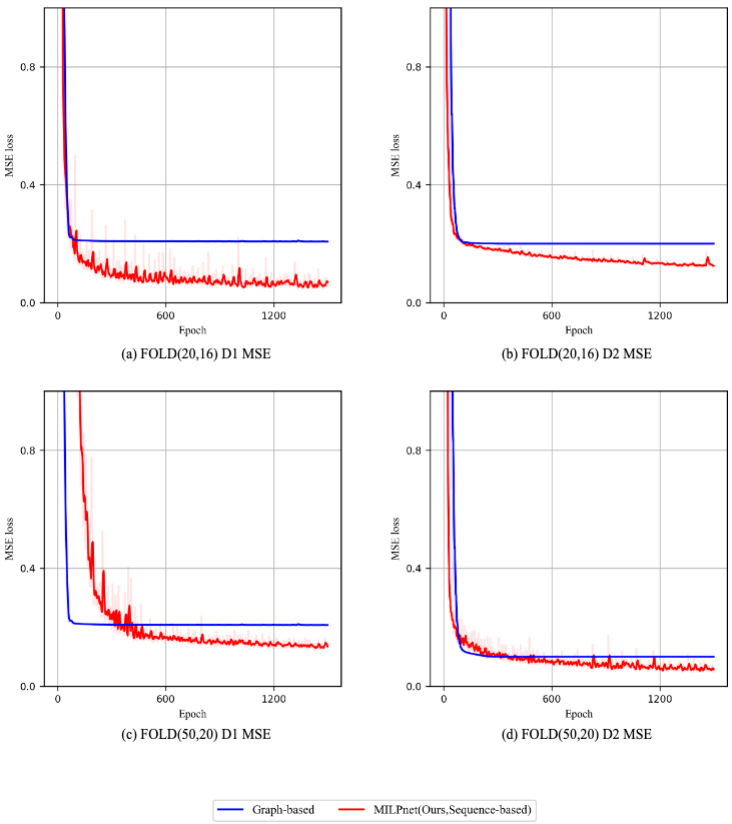

Figure 10: Representation experiments on optimal solution for FOLD20 and FOLD50 on D1 and D2 (details is shown in Appendix F). MILPnet approximates the solution mapping of Foldable MILP instances with smaller errors than graph-based method.

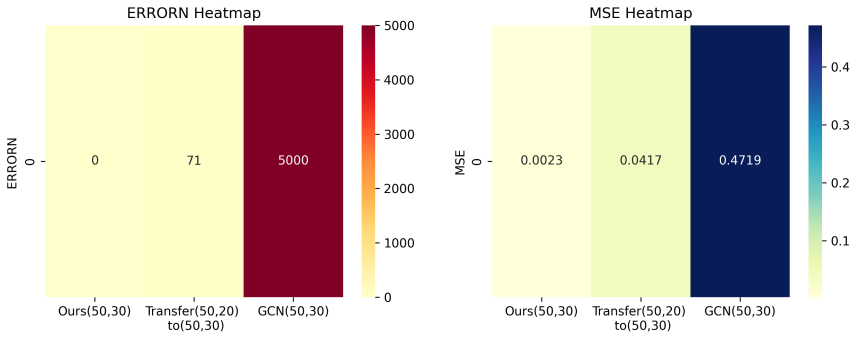

Figure 11: Cross-size adaptation

variables and 500 constraints, the number of the dataset are:training on 10000 instances, solving on 50 instances.

Table 13: Additional evaluations with more powerful GNN baselines, including GIN, PGN, and GraphGPS, on the Real world practical problems

	IP		SC		CA		FA	
	Time	Gap	Time	Gap	Time	Gap	Time	Gap
GIN	0.6254	0.0320	0.8223	0.6616	3.3065	0.7655	8.8688	0.7504
PGN	0.6023	0.1020	1.0492	0.4207	4.8369	1.0759	12.4009	0.7438
GraphGps	0.7324	0.0595	1.9202	0.4292	4.5980	1.0472	8.1973	0.8328
MILPnet(Ours)	**0.1864**	**0.0234**	**0.6915**	**0.3483**	**3.2300**	**0.7651**	**1.3773**	**0.3503**

C.2 ConPAS style Heterogeneous Variant on real-world instances solving

To address complex heterogeneous optimization problems in the real world,we train the hetergeneoous *MILPnet* as the solution representation predictors on SC problems and construct the trust region solving into three very large benchmarks from (Gleixner et al., 2021). The visualization of the solving results in terms of primal bound trajectories is shown in Figure 12.

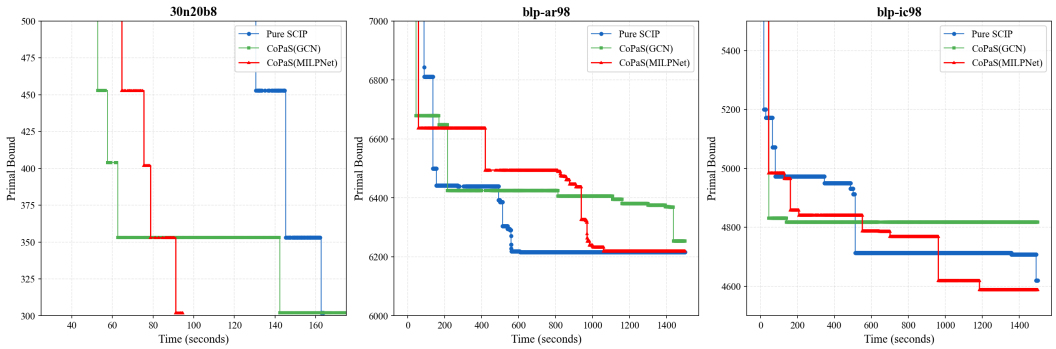

Figure 12: Primal bound iterations on very-large benchmarks solving with ConPAS(MILPnet)+SCIP and ConPAS(GCN)+SCIP

D GPU Analysis and Overall Performance Comparison

D.1 GPU memory analysis

Figure 13 visualizes the GPU usage during the training process.

D.2 Overall Performance Comparison

We conducted a comprehensive evaluation of various performance dimensions on the instances of FOLD300, and the results are shown in Figure 14.

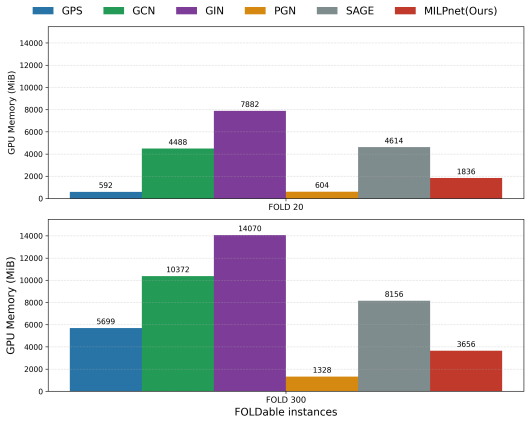

Figure 13: GPU memory usage on FOLD(20 ,*) to FOLD(300 ,*). **(The lower the better)**

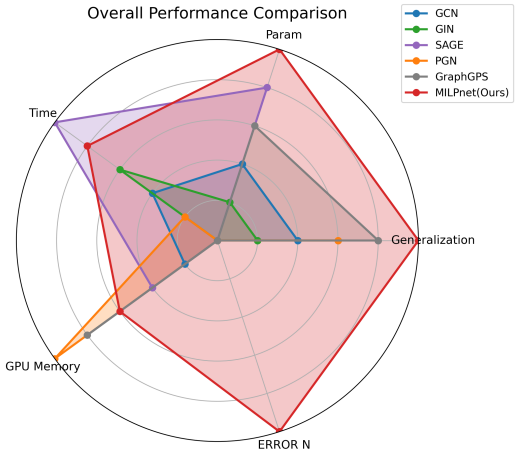

Figure 14: Overall performance comparisons on FOLD(300,*).**(The Broader the better)**

E PROOF OF THE SECTION 4.2 AND SECTION 4.3

We establish the results stated in Remark 4.2 and Section 4.3, where the former follows from Theorem 5 and the latter from Theorem 6 as follows.

Theorem 5 (**Padding Equivalence**). *Define the topological space before padding as:* $H^{MILP0} = ((H^{cons})^m \cup H^{Var}) \times I \times H^{obj}$ *and the padded topological space as* H^{MILP}. H^{MILP} *and* H^{MILP0} *are homeomorphic (topologically equivalent):*

$$H^{MILP} \cong H^{MILP0} \tag{13}$$

Proof. Define f as follows:

$$f\left((h_c, h_v, i, h_o)\right) = \left(h_c, \left(h_v, \underbrace{0, \ldots, 0}_{k \text{ times}}\right), \left(i, \underbrace{0, \ldots, 0}_{k \text{ times}}\right), \left(h_o, \underbrace{0, \ldots, 0}_{k \text{ times}}\right)\right),$$

where:

- $h_c \in (H^{\text{cons}})^m$,
- $h_v \in H^{\text{Var}}$,
- $i \in I$,
- $h_o \in H^{\text{obj}}$,
- $0, \ldots, 0 \in \{0\}^k$ are the padded zero dimensions.

Define f^{-1} as:

$$f^{-1}\left(\left(h_c, \left(h_v, \underbrace{0, \ldots, 0}_{k \text{ times}}\right), \left(i, \underbrace{0, \ldots, 0}_{k \text{ times}}\right), \left(h_o, \underbrace{0, \ldots, 0}_{k \text{ times}}\right)\right)\right) = (h_c, h_v, i, h_o).$$

Subsequently, we introduce **(i)** and **(ii)**, which are instrumental in establishing the main theorem.

(i) f is Bijective

Proof. f **is Injectivity:** Suppose $f(h_1) = f(h_2)$ for $h_1, h_2 \in H^{\text{MILP0}}$. Then,

$$f(h_1) = f(h_2) \implies (h_{c1}, (h_{v1}, 0, \ldots, 0), (i_1, 0, \ldots, 0), (h_{o1}, 0, \ldots, 0)) \tag{14}$$

$$= (h_{c2}, (h_{v2}, 0, \ldots, 0), (i_2, 0, \ldots, 0), (h_{o2}, 0, \ldots, 0)). \tag{15}$$

This equality implies:

$$h_{c1} = h_{c2}, \quad h_{v1} = h_{v2}, \quad i_1 = i_2, \quad h_{o1} = h_{o2}.$$

Therefore, $h_1 = h_2$, establishing injectivity.

f **is Surjectivity:** For any $h' \in H^{\text{MILP}}$, suppose $h' = (h_c, (h'_v, p_v), (i', p_i), (h'_o, p_o))$, where $p_v, p_i, p_o \in \{0\}^k$. Then, there exists $h \in H^{\text{MILP0}}$ such that:

$$h = (h_c, h'_v, i', h'_o).$$

Applying f to h, we obtain:

$$f(h) = (h_c, (h'_v, 0, \ldots, 0), (i', 0, \ldots, 0), (h'_o, 0, \ldots, 0)) = h'.$$

Thus, f is surjective.

(ii) f and f^{-1} are both continuous *Proof.* Both H^{MILP0} and H^{MILP} are equipped with the product topology. In the product topology, a function is continuous if and only if each of its component functions is continuous.

Continuity of f: The mapping f involves embedding each component of H^{MILP0} into a higher-dimensional space by appending zero vectors. Each such embedding is continuous because it is defined by coordinate-wise inclusion and fixed assignments (adding zeros). Specifically:

$$f_i : H_i \to H_i \times \{0\}^k$$

is continuous for each component $H_i \in \{H^{\text{cons}}, H^{\text{Var}}, I, H^{\text{obj}}\}$.

Continuity of f^{-1}: The inverse mapping f^{-1} involves projecting each padded component back to its original space by removing the appended zero vectors. Projection maps in the product topology are continuous. Specifically:

$$f_i^{-1} : H_i \times \{0\}^k \to H_i$$

is continuous for each component H_i.

Drawing upon the results presented in **(i)** and **(ii)**, the f is bijective and both f and f^{-1} are continuous, f is a homeomorphism. Therefore, the topological spaces H^{MILP} and H^{MILP0} are homeomorphic:

$$H^{\text{MILP}} \cong H^{\text{MILP0}}.$$

□

Theorem 6 (Constraint Permutation Invariance). *Let* $\left(H_1^{cons}, H_2^{cons}, \ldots, H_m^{cons}, I, H^{Var}, H^{obj}\right)$ *be topological spaces corresponding respectively to the* m *constraint feature spaces* H_i^{cons}*, the integer-index space* I'*, the variable-bounds space* $H^{Var'}$*, and the objective-coefficient space* $H^{obj'}$*. For any permutation* σ *on the index set* $\{1, 2, \ldots, m, \text{'}I\text{'}, \text{'}Var\text{'}, \text{'}obj\text{'}\}$*, their product spaces are homeomorphic:*

$$H_1^{cons} \times \cdots \times H_m^{cons} \times I' \times H^{Var'} \times H^{obj'} \cong \prod_{k \in \sigma(\{1,\ldots,m,I',Var',obj'\})} H^{(factor)_k}.$$

In other words, the topological structure of the full MILP-sequence feature space is invariant under permutation of its component spaces.

Proof The ordered product is

$$X = H_1^{\text{cons}} \times \cdots \times H_m^{\text{cons}} \times I' \times H^{\text{Var'}} \times H^{\text{obj'}},$$

Let

$$X_\sigma = \prod_{k \in \sigma(\{1,\ldots,m,\text{I'},\text{Var'},\text{obj'}\})} H^{(\text{factor})_k}$$

be an arbitrary permutation of the factors, where σ is a permutation of the index set.

We explicitly construct a *coordinate-exchange (or coordinate-reordering) map*

$$\Phi\colon X \longrightarrow X_\sigma.$$

Given a point

$$x = \left(h_1^{\text{cons}}, \ldots, h_m^{\text{cons}}, i', h^{\text{Var'}}, h^{\text{obj'}}\right) \in X,$$

where

$$h_i^{\text{cons}} \in H_i^{\text{cons}}, \quad i' \in I, \quad h^{\text{Var}} \in H^{\text{Var'}}, \quad h^{\text{obj'}} \in H^{\text{obj'}},$$

define $\Phi(x)$ by rearranging these coordinate components according to σ. Concretely, if σ sends the index 1 to position $\sigma(1)$, the index 2 to position $\sigma(2)$, etc., then

$$\Phi(x) = \underbrace{\left(h^{(\text{factor})}_{\text{the factor with index } \sigma^{-1}(1)}, \ldots\right)}_{\text{ordered according to } \sigma}.$$

In simpler terms, Φ reorders the factors $\left(h_1^{\text{cons}}, \ldots, h_m^{\text{cons}}, i, h^{\text{Var}}, h^{\text{obj}}\right)$ into the sequence $\left(\ldots\right)$ determined by σ.

Bijection. Φ is a *bijection* because:

- *Injective*: If $\Phi(x_1) = \Phi(x_2)$, then their coordinates in each position of the reordered product are identical. Since a product space comparison equates each factor, it follows that $x_1 = x_2$.
- *Surjective*: Given an arbitrary point $y \in X_\sigma$, we can "reverse reorder" its factors to form $x \in X$. By construction, $\Phi(x) = y$.

Because Φ is bijective and both Φ and Φ^{-1} are continuous, Φ is a *homeomorphism*. Hence

$$H_1^{\text{cons}} \times \cdots \times H_m^{\text{cons}} \times I' \times H^{\text{Var'}} \times H^{\text{obj'}} \cong \prod_{k \in \sigma(\{1,\ldots,m,\text{I'},\text{Var'},\text{obj'}\})} H^{(\text{factor})_k},$$

□

Theorem 7 (Variable Permutation Invariance). *Let* H^{MILP} *be the topological space of MILP-sequences defined in Section 4.3. For any permutation* π *on the variable indices* $\{1, 2, \ldots, n\}$*, the MILP-sequence space is homeomorphic under variable permutations:*

$$H^{MILP} \cong H_\pi^{MILP},$$

where H_π^{MILP} *denotes the space after permuting variable coordinates according to* π*. Consequently, the feasibility mapping* Φ_{feas}*, optimal objective value mapping* Φ_{obj}*, and optimal solution mapping* Φ_{solu} *are all invariant under variable permutation.*

Proof. We explicitly construct a *variable-coordinate reordering map*

$$\Psi\colon H^{\text{MILP}} \longrightarrow H_{\pi}^{\text{MILP}}.$$

Given an MILP-sequence

$$\mathbf{x} = [h_{\text{cons}}^{1}, \ldots, h_{\text{cons}}^{m}, h^{i'}, h^{\ell'}, h^{\mathfrak{V}'}, h^{c'}] \in H^{\text{MILP}},$$

where each component is a vector in $\mathbb{R}^{n+2}$, we define $\Psi(\mathbf{x})$ by applying the coordinate permutation to each token:

For each token $h = (h_1, \ldots, h_n, h_{n+1}, h_{n+2}) \in \mathbb{R}^{n+2}$ in the MILP-sequence, we define the coordinate permutation operator $P_\pi\colon \mathbb{R}^{n+2} \to \mathbb{R}^{n+2}$ by

$$P_\pi(h) = (h_{\pi(1)}, \ldots, h_{\pi(n)}, h_{n+1}, h_{n+2}),$$

where π permutes only the first n variable-related coordinates, leaving the last two padding coordinates unchanged. This operator applies uniformly to all tokens: constraint tokens h_i^{cons}, integer set token $h^{i'}$, variable bounds tokens $h^{\ell'}$ and $h^{\mathfrak{V}'}$, and objective token $h^{c'}$.

Then

$$\Psi(\mathbf{x}) = [P_\pi(h_{\text{cons}}^{1}), \ldots, P_\pi(h_{\text{cons}}^{m}), P_\pi(h^{i'}), P_\pi(h^{\ell'}), P_\pi(h^{\mathfrak{V}'}), P_\pi(h^{c'})] \in H_{\pi}^{\text{MILP}}.$$

Then we prove that Ψ is *bijective* and continuous:

1. **Bijection.** Ψ is a *bijection* because:
   - *Injective*: If $\Psi(\mathbf{x}_1) = \Psi(\mathbf{x}_2)$, then for each token, the permuted coordinates are identical. Since π is a bijection, the original coordinates must also be identical, hence $\mathbf{x}_1 = \mathbf{x}_2$.
   - *Surjective*: Given an arbitrary point $\mathbf{y} \in H_{\pi}^{\text{MILP}}$, we can apply the inverse permutation π^{-1} to each coordinate of each token to obtain $\mathbf{x} \in H^{\text{MILP}}$ such that $\Psi(\mathbf{x}) = \mathbf{y}$.
2. **Continuity.** Both Ψ and Ψ^{-1} are continuous because coordinate permutation is a continuous operation in the product topology of $\mathbb{R}^{n+2}$. Specifically, for each token space $\mathbb{R}^{n+2}$, the permutation map is a linear isomorphism, and the composition over all tokens preserves continuity in the product space $H^{\text{MILP}} \subset \mathbb{R}^{(m+4)(n+2)}$.

Therefore, Ψ is a *homeomorphism*, and

$$H^{\text{MILP}} \cong H_{\pi}^{\text{MILP}}.$$

□

Remark E.1 (Permutation Invariance)**.** Theorems 6 and 7 establish that H^{MILP} is invariant under both *constraint permutation* (reordering tokens) and *variable permutation* (reordering coordinates within tokens). These homeomorphisms ensure that different representations of the same MILP instance are topologically equivalent and define identical optimization problems. Consequently, the mappings Φ_{feas}, Φ_{obj}, and Φ_{solu} are invariant under both types of permutations, which is crucial for designing permutation-equivariant neural architectures.

F Proof of the Mappings.

We introduced the details of the MILP-sequence mapping definitions: with the defined topological space H^{MILP}, which encapsulates the MILP-sequence, we can define key mappings essential for analyzing MILP instances. These mappings assess feasibility, compute optimal objective values, and identify optimal solutions, providing a comprehensive toolkit for MILP analysis.

Definition 8. (Feasibility mapping by sequence) The feasibility mapping is a classification function that determines whether a sequence within H^{MILP} represents a feasible solution:

$$\Phi_{\text{feas}} : H^{\text{MILP}} \to \{0, 1\} \tag{16}$$

where $\Phi_{\text{feas}} = 1$ indicates that the MILP instance is feasible.

Definition 9. (Optimal objective value mapping by sequence) The optimal objective value mapping for each MILP instance is defined as:

$$\Phi_{\text{obj}} : H^{\text{MILP}} \to \mathbb{R} \cup \{\infty, -\infty\} \tag{17}$$

which projects feasible sequences to their respective optimal values.

Definition 10. (Optimal solution mapping by sequence) To simplify the discussion, we focus on settings where all components of the vectors ℓ and u are finite. This assumption ensures the existence of an optimal solution when the MILP problem is feasible. Consequently, we define a restricted subset of the MILP topological space, $\widetilde{H}^{\text{MILP}} \subset H^{\text{MILP}}$, which only has finite variable bounds. The optimal solution mapping for the MILP-sequence is defined as: For any $F \in \Phi_{\text{obj}}^{-1}(\mathbb{R})$, the MILP problem has a unique optimal solution with the smallest ℓ_2-norm. Let

$$\Phi_{\text{solu}} : \widetilde{H}^{\text{MILP}} \cap \Phi_{\text{feas}}^{-1}(1) \to \mathbb{R}^n \tag{18}$$

Then we prove the feature mappings of the MILP-sequence are measurable in the following theorems.

Theorem 11. ***The feasibility mapping for MILP-sequence is measurable.***

Proof The target space $\{0, 1\}$ is equipped with the discrete σ-algebra, where every subset is Borel. Specifically, the Borel sets in $\{0, 1\}$ are:

$$\mathcal{B}_{\{0,1\}} = \{\emptyset, \{0\}, \{1\}, \{0, 1\}\}.$$

We consider each possible Borel set $B \subseteq \{0, 1\}$ and examine $\Phi_{\text{feas}}^{-1}(B)$:

1. $B = \emptyset$:
$$\Phi_{\text{feas}}^{-1}(\emptyset) = \emptyset,$$
which is trivially a Borel set.
2. $B = \{1\}$:
$$\Phi_{\text{feas}}^{-1}(\{1\}) = \left\{ (x, h) \in H^{\text{MILP}} \,\middle|\, \text{the MILP instance is feasible} \right\}.$$
The feasibility of a MILP instance is determined by the existence of solutions that satisfy all linear constraints and integrality conditions. Specifically, it requires that there exists $x \in \mathbb{R}^n$ such that:
$$Ax \leq b, \quad \ell \leq x \leq u, \quad x_j \in \mathbb{Z}\ \forall j \in \mathcal{I},$$
where $\mathcal{I}$ is the set of indices corresponding to integer variables.
The set of feasible MILP instances can be expressed as the intersection of:
   - A finite union of closed half-spaces defined by the linear constraints $Ax \leq b$.
   - Closed intervals defined by the variable bounds $\ell \leq x \leq u$.
   - Discrete conditions $x_j \in \mathbb{Z}$ for integer variables.

   Since finite unions and intersections of closed sets are closed (hence Borel), and the discrete conditions correspond to countable intersections, $\Phi_{\text{feas}}^{-1}(\{1\})$ is a Borel set in the product topology of $\mathbb{R}^{(m+4)(n+2)} \times H^{\text{MILP}}$.
3. $B = \{0\}$:
$$\Phi_{\text{feas}}^{-1}(\{0\}) = \left\{ (x, h) \in H^{\text{MILP}} \,\middle|\, \text{the MILP instance is infeasible} \right\}.$$
The infeasibility set is the complement of the feasibility set:
$$\Phi_{\text{feas}}^{-1}(\{0\}) = \left(\Phi_{\text{feas}}^{-1}(\{1\})\right)^c.$$
Since $\Phi_{\text{feas}}^{-1}(\{1\})$ is a Borel set and the complement of a Borel set is also a Borel set, $\Phi_{\text{feas}}^{-1}(\{0\})$ is Borel.

4. $B = \{0, 1\}$:
$$\Phi_{\text{feas}}^{-1}(\{0, 1\}) = H^{\text{MILP}},$$
which is the entire space and hence a Borel set.

Since for every Borel set $B \subseteq \{0, 1\}$, the preimage $\Phi_{\text{feas}}^{-1}(B)$ is a Borel set in $\mathbb{R}^{(m+4)(n+2)} \times H^{\text{MILP}}$, the feasibility mapping Φ_{feas} is measurable. □

Remark F.1. *The measurability of Φ_{feas} is crucial for ensuring that probabilistic and statistical analyses involving MILP instances are well-defined. Since Φ_{feas} maps measurable spaces to a discrete space with a simple σ-algebra, its measurability guarantees that feasibility can be reliably incorporated into broader measure-theoretic frameworks.*

Remark F.2. *Both the domain H^{MILP} and the codomain $\{0, 1\}$ are equipped with their respective σ-algebras. The domain utilizes the product topology, and H^{MILP} itself is a product of measurable spaces as defined earlier. The codomain $\{0, 1\}$ employs the discrete σ-algebra, where all subsets are measurable.*

Theorem 12. ***The optimal objective value mapping for MILP-sequence is measurable.***

Proof To prove that the optimal objective value mapping $\Phi_{\text{obj}} : H^{\text{MILP}} \to \mathbb{R} \cup \{\infty, -\infty\}$ is measurable, we need to demonstrate that for every Borel set $B \subseteq \mathbb{R} \cup \{\infty, -\infty\}$, the preimage $\Phi_{\text{obj}}^{-1}(B)$ is a Borel set in $\mathbb{R}^{(m+4)(n+2)} \times H^{\text{MILP}}$.

The codomain $\mathbb{R} \cup \{\infty, -\infty\}$ can be equipped with the extended real line topology, where the Borel σ-algebra is generated by the open intervals in $\mathbb{R}$ along with the points $\{\infty\}$ and $\{-\infty\}$. The Borel sets in $\mathbb{R} \cup \{\infty, -\infty\}$ include:

1. $B \subseteq \mathbb{R}$
2. B contains ∞ and/or $-\infty$

We consider each category of Borel sets in $\mathbb{R} \cup \{\infty, -\infty\}$ and examine $\Phi_{\text{obj}}^{-1}(B)$.

1. $B \subseteq \mathbb{R}$:
$$\Phi_{\text{obj}}^{-1}(B) = \left\{ (x, h) \in H^{\text{MILP}} \;\middle|\; \text{the optimal objective value of the MILP instance is in } B \right\}.$$
Assuming that the MILP's optimal objective value is determined by a continuous optimization process (which holds under certain regularity conditions, such as linearity of the objective function and constraints), Φ_{obj} can be considered a continuous function on the feasible set. Therefore, the preimage of any Borel set $B \subseteq \mathbb{R}$ under Φ_{obj} is a Borel set in the domain.
2. B contains ∞ and/or $-\infty$:
$$\Phi_{\text{obj}}^{-1}(B) = \left\{ (x, h) \in H^{\text{MILP}} \;\middle|\; \Phi_{\text{obj}}(x, h) \in B \right\}.$$
The inclusion of ∞ or $-\infty$ typically corresponds to the infeasibility or unboundedness of the MILP instance:
   - If $\Phi_{\text{obj}}(x, h) = \infty$, the MILP instance is unbounded above.
   - If $\Phi_{\text{obj}}(x, h) = -\infty$, the MILP instance is unbounded below.

   These conditions define specific subsets of the domain:
$$\Phi_{\text{obj}}^{-1}(\{\infty\}) = \left\{ (x, h) \in H^{\text{MILP}} \;\middle|\; \text{MILP is unbounded above} \right\},$$
   and
$$\Phi_{\text{obj}}^{-1}(\{-\infty\}) = \left\{ (x, h) \in H^{\text{MILP}} \;\middle|\; \text{MILP is unbounded below} \right\}.$$
   Assuming that the conditions for unboundedness are also defined by Borel sets (similar to feasibility), these preimages are Borel sets in the domain.

Since for every Borel set $B \subseteq \mathbb{R} \cup \{\infty, -\infty\}$, the preimage $\Phi_{\text{obj}}^{-1}(B)$ is a Borel set in $\mathbb{R}^{(m+4)(n+2)} \times H^{\text{MILP}}$, the mapping Φ_{obj} is measurable. □

Before we give the proof of the mensurability of the optimal solution mapping for the MILP-sequence,we first introduce the Jankov-von Neumann Measurable Selection Theorem.

Theorem 13 (Jankov-von Neumann Measurable Selection Theorem,(Dubins & Savage, 2014; Neumann, 1936)**).** *Let $(X, \mathcal{A})$ and $(Y, \mathcal{B})$ be measurable spaces, and let $S : X \to 2^Y$ be a measurable set-valued map such that for all $x \in X$, $S(x)$ is non-empty and closed in Y. Then, there exists a measurable function $f : X \to Y$ such that $f(x) \in S(x)$ for all $x \in X$.*

Remark F.3. *The **Jankov-von Neumann Measurable Selection Theorem** provides a crucial guarantee in measure theory and its applications. Given a measurable space X and a set-valued mapping $A : X \to 2^Y$ where each $A(x)$ is a non-empty set, the theorem ensures the existence of a measurable function f that selects an element from each $A(x)$ in a measurable manner. Specifically, for almost every $x \in X$, the function f assigns a value $f(x)$ that belongs to the set $A(x)$. This result is particularly useful in areas such as optimization, probability theory, and economics, where selecting measurable choices from a set of feasible options is essential.*

Then we prove the measurblity of the optimal solution mapping for the MILP-sequence.

Theorem 14. ***The optimal solution mapping for the MILP-sequence is measurable.***

Proof. This part proves the optimal solution mapping for the MILP-sequence is measurable. To prove that the optimal solution mapping

$$\Phi_{\text{solu}} : \widetilde{H}^{\text{MILP}} \cap \Phi_{\text{feas}}^{-1}(1) \to \mathbb{R}^n$$

is measurable, we need to demonstrate that for every Borel set $B \subseteq \mathbb{R}^n$, the preimage

$$\Phi_{\text{solu}}^{-1}(B)$$

is a Borel set in H^{MILP}.

Consider the mapping Φ_{solu} as a selection function that assigns to each feasible MILP instance its unique optimal solution with the smallest ℓ_2-norm. Formally, for each

$$(x, h) \in \widetilde{H}^{\text{MILP}} \cap \Phi_{\text{feas}}^{-1}(1),$$

there exists at least one $x^* \in \mathbb{R}^n$ such that x^* is an optimal solution. We aim to select a unique x^* for each instance in a measurable manner. With Theorem 13, for each

$$(x, h) \in \widetilde{H}^{\text{MILP}} \cap \Phi_{\text{feas}}^{-1}(1),$$

the set of optimal solutions

$$S(x, h) = \{x^* \in \mathbb{R}^n \mid x^* \text{ is an optimal solution for } (x, h)\}$$

is non-empty and closed, then there exists a measurable selection function

$$\Phi_{\text{solu}} : \widetilde{H}^{\text{MILP}} \cap \Phi_{\text{feas}}^{-1}(1) \to \mathbb{R}^n$$

such that

$$\Phi_{\text{solu}}(x, h) \in S(x, h)$$

for all

$$(x, h) \in \widetilde{H}^{\text{MILP}} \cap \Phi_{\text{feas}}^{-1}(1).$$

Then, we prove the Non-emptiness and Cloasedness of $\widetilde{H}^{\text{MILP}} \cap \Phi_{\text{feas}}^{-1}(1)$, detailed as:

1. **Non-emptiness:** By definition,
$$\widetilde{H}^{\text{MILP}} \cap \Phi_{\text{feas}}^{-1}(1)$$
consists of MILP instances that are feasible and have finite bounds, ensuring that an optimal solution exists. Therefore, $S(x, h)$ is non-empty for all
$$(x, h) \in \widetilde{H}^{\text{MILP}} \cap \Phi_{\text{feas}}^{-1}(1).$$

2. **Closedness:** The set of optimal solutions $S(x,h)$ is closed in $\mathbb{R}^n$. This is because optimal solutions to MILP problems, defined by linear constraints and objective functions, form closed sets under standard topologies.

Given that both the closedness and non-emptiness conditions are satisfied, Theorem 13 ensures the existence of a measurable selection function Φ_{solu}. Since Φ_{solu} is a measurable selection function by the theorem, for any Borel set $B \subseteq \mathbb{R}^n$,

$$\Phi_{\text{solu}}^{-1}(B) = \{(x,h) \in H^{\text{MILP}} \mid \Phi_{\text{solu}}(x,h) \in B\}$$

is a Borel set in H^{MILP}. Therefore, the mapping Φ_{solu} is measurable. □

After establishing the measurability of the feasibility, optimal objective value, and optimal solution mappings, we define the corresponding measurable mapping sets for each of these mappings as follows:

Definition 15. (Measurable Mapping Set for Feasibility Mapping) The **Feasibility Mapping Set** consists of all measurable functions

$$\Phi_{\text{feas}} : H^{\text{MILP}} \to \{0,1\},$$

where $\Phi_{\text{feas}}(x,h) = 1$ indicates that the MILP instance defined by (x,h) is feasible, and $\Phi_{\text{feas}}(x,h) = 0$ indicates infeasibility. Formally, the set is defined as:

$$\mathcal{F}_{\text{feas}}^{\text{MILP}} = \left\{ \Phi_{\text{feas}} : H^{\text{MILP}} \to \{0,1\} \;\middle|\; \Phi_{\text{feas}} \text{ is measurable} \right\}.$$

Definition 16 (Measurable Mapping Set for Optimal Objective Value Mapping)**.** The **Optimal Objective Value Mapping Set** comprises all measurable functions

$$\Phi_{\text{obj}} : H^{\text{MILP}} \to \mathbb{R} \cup \{\infty, -\infty\},$$

which assign to each MILP instance (x,h) its optimal objective value. Specifically,

$$\Phi_{\text{obj}}(x,h) = \begin{cases} c^T x^* & \text{if the MILP instance is feasible and bounded,} \\ \infty & \text{if the MILP instance is unbounded above,} \\ -\infty & \text{if the MILP instance is unbounded below.} \end{cases}$$

Formally, the set is defined as:

$$\mathcal{F}_{\text{obj}}^{\text{MILP}} = \left\{ \Phi_{\text{obj}} : H^{\text{MILP}} \to \mathbb{R} \cup \{\infty, -\infty\} \;\middle|\; \Phi_{\text{obj}} \text{ is measurable} \right\}.$$

Definition 17 (Measurable Mapping Set for Optimal Solution Mapping)**.** The **Optimal Solution Mapping Set** consists of all measurable functions

$$\Phi_{\text{solu}} : \widetilde{H}^{\text{MILP}} \cap \Phi_{\text{feas}}^{-1}(1) \to \mathbb{R}^n,$$

which assign to each feasible and bounded MILP instance (x,h) its unique optimal solution x^* with the smallest ℓ_2-norm. Formally, the set is defined as:

$$\mathcal{F}_{\text{solu}}^{\text{MILP}} = \left\{ \Phi_{\text{solu}} : \widetilde{H}^{\text{MILP}} \cap \Phi_{\text{feas}}^{-1}(1) \to \mathbb{R}^n \;\middle|\; \Phi_{\text{solu}} \text{ is measurable} \right\}.$$

G THE PROOF OF THE SECTION 5.2.

Firstly, theorem Lusin is presented before the proof in this section.

Theorem 18 (Lusin's Theorem,(Mammeri, 2019))**.** *Let $f : \mathbb{R} \to \mathbb{R}$ be a measurable function on a measurable set $E \subset \mathbb{R}$ with finite measure. For every $\epsilon > 0$, there exists a closed set $C \subset E$ such that the measure of $E \setminus C$ is less than ϵ, and f restricted to C is continuous.*

Secondly, for the probability measure used in Theorems 2–4 we would like give the Remark G.1 to clarify the probability using:

Remark G.1 (On the Probability Measure)**.** The probability $P(\cdot)$ in Theorems 2–4 accounts for the randomness in neural network training, including random initialization and stochastic optimization (SGD). Specifically, P is the probability measure over the space of trained networks induced by the random training process. This formulation aligns with the Probably Approximately Correct learning. For a fixed trained network F_{HYA}, the probability can be interpreted as the empirical error rate on the finite dataset D.

Then we give the proof of the theorems in the Section 5.2.

G.1 Proof and Corollary on Theorem 2

Proof of Theorem 2 We leverage the measurability of the feasibility mapping Φ_{feas}, the Jankov-von Neumann Measurable Selection Theorem, and Lusin's Theorem to construct a neural network F_{HYA} that approximates Φ_{feas} with high accuracy on the finite dataset D.

From our earlier definitions in Definition 15, $\Phi_{\text{feas}} : H^{\text{MILP}} \to \{0, 1\}$ is measurable. This ensures that Φ_{feas} is compatible with measure-theoretic frameworks. Lusin's Theorem states that for any measurable function and any $\delta > 0$, there exists a compact subset where the function is continuous and the measure of the complement is less than δ. However, since D is a finite dataset, we can consider the discrete measure where each point in D has an equal probability mass.

Given the finiteness of D, Lusin's Theorem trivially holds as we can define $\delta = \epsilon$ and select the entire dataset D as the compact subset where Φ_{feas} is continuous (since all functions on finite sets are continuous).

By the Universal Approximation Theorem, Since our MILPnet is an architecture that combines at least one-layer feedforward network structure with activation functions, it can approximate any continuous function on a compact subset to arbitrary accuracy. Since D is finite, and Φ_{feas} is effectively continuous on D, there exists a neural network $F_{\text{HYA}} \in \mathcal{F}_{\text{HYA}}^{\text{MILPnet}}$ that satisfies:

$$|F_{\text{HYA}}(x) - \Phi_{\text{feas}}(x)| < \frac{1}{2}, \quad \forall x \in D.$$

This ensures that:

$$\mathbb{I}_{F_{\text{HYA}}}(x) = \begin{cases} 1 & \text{if } F_{\text{HYA}}(x) > \frac{1}{2}, \\ 0 & \text{otherwise,} \end{cases}$$

matches $\Phi_{\text{feas}}(x)$ exactly for all $x \in D$. Since D is finite, the probability P can be interpreted as a uniform distribution over D. Given that F_{HYA} correctly classifies all $x \in D$, we have:

$$P\left(\mathbb{I}_{F_{\text{HYA}}(x)>\frac{1}{2}} \neq \Phi_{\text{feas}}(x)\right) = 0 < \epsilon.$$

Thus, the constructed neural network F_{HYA} satisfies the required condition for the theorem. □

Remark G.2. *While the above steps suffice for a finite dataset, the framework can be extended using the Jankov-von Neumann Measurable Selection Theorem for more general settings. This theorem ensures the existence of a measurable selection function that can be approximated by neural networks even in infinite-dimensional spaces, provided the feasibility mapping satisfies the necessary measurability and closedness conditions. However, for the scope of this theorem with a finite dataset D, the construction above is sufficient to guarantee the existence of the desired neural network F_{HYA}.*

Then we have corollary on the infinite dataset for feasibility mapping:

Corollary 1 (Extension to infinite dataset)**.** Let $D \subset H^{\text{MILP}}$ be an infinite or continuous dataset with a finite measure $\mu(D) < \infty$. For any $\epsilon > 0$, there exists a neural network $F_{\text{HYA}} \in \mathcal{F}_{\text{HYA}}^{\text{MILPnet}}$ such that:

$$P\left(\mathbb{I}_{F_{\text{HYA}}(x)>\frac{1}{2}} \neq \Phi_{\text{feas}}(x)\right) < \epsilon, \quad \forall x \in D, \tag{19}$$

where x is the MILP-sequence, and $\Phi_{\text{feas}}(x)$ is the feasibility mapping of the MILP instance.

Proof. We have proven that the feasibility mapping $\Phi_{\text{feas}} : H^{\text{MILP}} \to \{0, 1\}$ is assumed to be measurable on D in Theorem B.1.

By **Lusin's Theorem**, for the measurable function Φ_{feas} and for any $\epsilon > 0$, there exists a compact (closed and bounded) subset $C \subset D$ such that:

$$\mu(D \setminus C) < \epsilon$$

and Φ_{feas} restricted to C is continuous:

$$\Phi_{\text{feas}}|_C : C \to \{0, 1\} \text{ is continuous.}$$

Since Φ_{feas} is a simple indicator function, its continuity on C implies that C avoids the boundary cases where the feasibility of the MILP instances changes.

Given that Φ_{feas} is continuous on C, by the Universal Approximation Theorem, there exists a neural network $F_{\text{HYA}} \in \mathcal{F}_{\text{HYA}}^{\text{MILPnet}}$ that approximates the indicator function $\mathbb{I}_{\Phi_{\text{feas}}(x)}$ to within an error less than $\frac{1}{2}$ on C. Specifically:

$$\left|F_{\text{HYA}}(x) - \mathbb{I}_{\Phi_{\text{feas}}(x)}\right| < \frac{1}{2}, \quad \forall x \in C$$

This implies that:

$$\mathbb{I}_{F_{\text{HYA}}(x) > \frac{1}{2}} \iff \mathbb{I}_{\Phi_{\text{feas}}(x)} = 1, \quad \forall x \in C$$

Thus, the neural network F_{HYA} correctly classifies the feasibility of MILP instances in C. Consider the probability that the classification error occurs:

$$P\left(\mathbb{I}_{F_{\text{HYA}}(x) > \frac{1}{2}} \neq \Phi_{\text{feas}}(x)\right)$$

This event can only occur if $x \in D \setminus C$, since for $x \in C$, the classification is guaranteed to be correct. Therefore:

$$P\left(\mathbb{I}_{F_{\text{HYA}}}(x) > \frac{1}{2} \neq \Phi_{\text{feas}}(x)\right) \leq \mu(D \setminus C) < \epsilon$$

Thus, the probability that F_{HYA} misclassifies any $x \in D$ is bounded by ϵ. By constructing F_{HYA} using Lusin's Theorem to ensure continuity on a large compact subset C of D, and then applying the Universal Approximation Theorem to approximate the feasibility indicator function on C, we have established the existence of a neural network within $\mathcal{F}_{\text{HYA}}^{\text{MILPnet}}$ that satisfies the desired probabilistic bound for the classification task on infinite or continuous datasets D. □

G.2 Proof and corollary of Theorem 3

Proof of Theorem 3 To prove the theorem, we leverage the **Lusin's Theorem** alongside the Universal Approximation Theorem for neural networks. The proof is divided into two parts corresponding to the classification and regression problems.

1. Classification Problem:

We aim to construct a neural network $F_{\text{HYA},1}$ that accurately classifies whether the objective value $\Phi_{\text{obj}}(x)$ is finite for all $x \in D$.

First, we have proven that the feature mapping $\Phi_{\text{obj}} : H^{\text{MILP}} \to \mathbb{R} \cup \{\infty\}$ is measurable. By **Lusin's Theorem**, for any measurable function f defined on a measurable set with finite measure, and for any $\epsilon > 0$, there exists a closed set $C \subset D$ such that:

$$\mu(D \setminus C) < \epsilon$$

and f restricted to C is continuous. Since D is finite, the measure $\mu(D)$ is finite, and thus Lusin's Theorem is applicable. Therefore, there exists a subset $C \subset D$ where Φ_{obj} is continuous.

Given that Φ_{obj} is continuous on C, by the Universal Approximation Theorem, there exists a neural network $F_{\text{HYA},1} \in \mathcal{F}_{\text{HYA}}^{\text{MILPnet}}$ that approximates the indicator function $\mathbb{I}_{\Phi_{\text{obj}}(x) \in \mathbb{R}}$ to within an error less than ϵ on C. Specifically:

$$\left|F_{\text{HYA},1}(x) - \mathbb{I}_{\Phi_{\text{obj}}(x) \in \mathbb{R}}\right| < \frac{1}{2}, \quad \forall x \in C$$

Since $\mu(D \setminus C) < \epsilon$, the probability that $F_{\text{HYA},1}$ misclassifies any $x \in D$ is less than ϵ:

$$P\left(\mathbb{I}_{F_{\text{HYA},1}(x)>\frac{1}{2}} \neq \mathbb{I}_{\Phi_{\text{obj}}(x)\in\mathbb{R}}\right) < \epsilon, \quad \forall x \in D$$

2. Regression problems:

Next, we construct a neural network $F_{\text{HYA},2}$ to predict the objective value $\Phi_{\text{obj}}(x)$ with an error less than δ for all $x \in D$ where $\Phi_{\text{obj}}(x)$ is finite.

We have proven that the Φ_{obj} is measurable in Theorem B.2. By **Lusin's Theorem**, for the regression task, there exists a closed subset $C' \subset D \cap \Phi_{\text{obj}}^{-1}(\mathbb{R})$ such that:

$$\mu\left((D \cap \Phi_{\text{obj}}^{-1}(\mathbb{R})) \setminus C'\right) < \epsilon$$

and Φ_{obj} is continuous on C'.

By the Universal Approximation Theorem, there exists a neural network $F_{\text{HYA},2} \in \mathcal{F}_{\text{HYA}}^{\text{MILPnet}}$ that approximates Φ_{obj} to within an error δ on C':

$$|F_{\text{HYA},2}(x) - \Phi_{\text{obj}}(x)| < \delta, \quad \forall x \in C'$$

Since the measure of the complement set is less than ϵ, the probability that the prediction error exceeds δ is bounded by ϵ:

$$P\left(|F_{\text{HYA},2}(x) - \Phi_{\text{obj}}(x)| > \delta\right) < \epsilon, \quad \forall x \in D \cap \Phi_{\text{obj}}^{-1}(\mathbb{R})$$

By constructing $F_{\text{HYA},1}$ and $F_{\text{HYA},2}$ using Lusin's Theorem to ensure measurability and continuity on large subsets, and then applying the Universal Approximation Theorem to approximate the respective functions, we have established the existence of neural networks within $\mathcal{F}_{\text{HYA}}^{\text{MILPnet}}$ that satisfy the desired probabilistic bounds for both classification and regression tasks on the finite dataset D. □

Then we give the corollary on the infinite dataset for optimal objective mapping as follows:

Corollary 2 (Extension to Compact Infinite Sets)**.** Let $K \subset H^{\text{MILP}}$ be a compact subset equipped with the measure $\mu_{H^{\text{MILP}}}$ defined in Section 4.2. Define the probability measure P on K by normalizing: $P(A) = \frac{\mu_{H^{\text{MILP}}}(A)}{\mu_{H^{\text{MILP}}}(K)}$ for any measurable set $A \subset K$.

For any $\epsilon, \delta > 0$, there exist two neural networks $F_{\text{HYA},1}, F_{\text{HYA},2} \in \mathcal{F}_{\text{HYA}}^{\text{MILPnet}}$ such that:

1. Classification of finite objective values:

$$P\left(\mathbb{I}_{F_{\text{HYA},1}(x)>\frac{1}{2}} \neq \mathbb{I}_{\Phi_{\text{obj}}(x)\in\mathbb{R}}\right) < \epsilon, \quad \forall x \in K \tag{20}$$

2. Regression of objective values:

$$P\left(|F_{\text{HYA},2}(x) - \Phi_{\text{obj}}(x)| > \delta\right) < \epsilon, \quad \forall x \in K \cap \Phi_{\text{obj}}^{-1}(\mathbb{R}) \tag{21}$$

Proof. The proof parallels Theorem 3, replacing the counting measure on finite D with the probability measure P on compact K.

1. Classification Problem.

Since $\Phi_{\text{obj}} : H^{\text{MILP}} \to \mathbb{R} \cup \{\infty\}$ is measurable and K is compact with $\mu_{H^{\text{MILP}}}(K) < \infty$, we apply Lusin's Theorem.

For any $\epsilon > 0$, there exists a closed set $C \subset K$ such that:

$$P(K \setminus C) = \frac{\mu_{H^{\text{MILP}}}(K \setminus C)}{\mu_{H^{\text{MILP}}}(K)} < \frac{\epsilon}{2}$$

and $\Phi_{\text{obj}}|_C$ is continuous. By the Universal Approximation Theorem, there exists $F_{\text{HYA},1} \in \mathcal{F}_{\text{HYA}}^{\text{MILPnet}}$ such that:

$$\sup_{x\in C} \left|F_{\text{HYA},1}(x) - \mathbb{I}_{\Phi_{\text{obj}}(x)\in\mathbb{R}}\right| < \frac{1}{4}$$

This ensures that for all $x \in C$:

$$\mathbb{I}_{F_{\text{HYA},1}(x)>\frac{1}{2}} = \mathbb{I}_{\Phi_{\text{obj}}(x)\in\mathbb{R}}$$

The set of misclassified points is contained in $K \setminus C$, therefore:

$$P\left(\mathbb{I}_{F_{\text{HYA},1}(x)>\frac{1}{2}} \neq \mathbb{I}_{\Phi_{\text{obj}}(x)\in\mathbb{R}}\right) \leq P(K \setminus C) < \epsilon$$

2. Regression Problem. Let $K_{\text{finite}} = K \cap \Phi_{\text{obj}}^{-1}(\mathbb{R})$. Define the conditional probability measure on K_{finite} by:

$$P_{\text{finite}}(A) = \frac{\mu_{H^{\text{MILP}}}(A)}{\mu_{H^{\text{MILP}}}(K_{\text{finite}})}, \quad A \subset K_{\text{finite}}$$

By Lusin's Theorem applied to Φ_{obj} on K_{finite}, for any $\epsilon > 0$, there exists a closed set $C' \subset K_{\text{finite}}$ such that:

$$P_{\text{finite}}(K_{\text{finite}} \setminus C') < \frac{\epsilon}{2}$$

and $\Phi_{\text{obj}}|_{C'}$ is continuous. By the Universal Approximation Theorem, there exists $F_{\text{HYA},2} \in \mathcal{F}_{\text{HYA}}^{\text{MILPnet}}$ such that:

$$\sup_{x\in C'} |F_{\text{HYA},2}(x) - \Phi_{\text{obj}}(x)| < \delta$$

Therefore:

$$P_{\text{finite}}\left(|F_{\text{HYA},2}(x) - \Phi_{\text{obj}}(x)| > \delta\right) \leq P_{\text{finite}}(K_{\text{finite}} \setminus C') < \epsilon$$

□

G.3 Proof and the corollary of Theorem 4

Proof of Theorem 4 Since D is finite, let us denote it as:

$$D = \{x_1, x_2, \ldots, x_n\}$$

for some integer $n \geq 1$. For each $x_i \in D$, $\Phi_{\text{solu}}(x_i)$ is a well-defined finite solution in $\mathbb{R}^n$.

The Universal Approximation Theorem states that a feedforward neural network with at least one hidden layer and a sufficient number of neurons can approximate any continuous function on compact subsets of $\mathbb{R}^n$ to any desired degree of accuracy, provided the activation function is non-linear (e.g., Sigmoid, ReLU).

Given that D is finite, it is trivially compact. Therefore, there exists a neural network $F_{\text{HYA},W}$ that can approximate the mapping Φ_{solu} on D with arbitrary precision. Specifically, for each $x_i \in D$, we can ensure:

$$\|F_{\text{HYA},W}(x_i) - \Phi_{\text{solu}}(x_i)\| < \delta$$

by appropriately choosing the network architecture and weights W.

Since D is finite, the probability P can be interpreted over a uniform distribution or any probability measure defined on D. However, because we have constructed $F_{\text{HYA},W}$ such that the approximation error is less than δ for every $x \in D$, the event

$$\|F_{\text{HYA},W}(x) - \Phi_{\text{solu}}(x)\| > \delta$$

does not occur for any $x \in D$. Therefore:

$$P\left(\|F_{\text{HYA},W}(x) - \Phi_{\text{solu}}(x)\| > \delta\right) = 0 < \epsilon$$

for any $\epsilon > 0$.

By the Universal Approximation Theorem, we can construct a neural network $F_{\text{HYA},W}$ that approximates the solution mapping Φ_{solu} on the finite dataset D with an error less than δ for all $x \in D$. Consequently, the probability that the approximation error exceeds δ is zero, which is trivially less than any $\epsilon > 0$. This establishes the existence of such a neural network within $\mathcal{F}_{\text{HYA},V}^{\text{MILPnet}}$. □

Then we have the corollary on the infinite dataset:

Corollary 3 (Extension to infinite dataset)**.** Let $D \subset \Phi_{\text{obj}}^{-1}(\mathbb{R}) \subset H^{\text{MILP}}$ be an infinite dataset with a finite measure $\mu(D) < \infty$. For any $\epsilon, \delta > 0$, there exists a neural network $F_{\text{HYA},W} \in \mathcal{F}_{\text{HYA},W}^{\text{MILPnet}}$ such that:

$$P\left(\|F_{\text{HYA},W}(x) - \Phi_{\text{solu}}(x)\| > \delta\right) < \epsilon, \quad \forall x \in D, \tag{22}$$

where P denotes the probability measure on D.

Proof. To extend the theorem to infinite datasets, we employ **Lusin's Theorem** in conjunction with the Universal Approximation Theorem.

Assume D is equipped with a probability measure μ such that $\mu(D) = 1$ (without loss of generality, as we can normalize the measure). Also, we have proven that the solution mapping $\Phi_{\text{solu}} : H^{\text{MILP}} \to \mathbb{R}^n$ is measurable on D before.

By Lusin's Theorem, for the measurable function Φ_{solu} and for any $\epsilon > 0$, there exists a compact (closed and bounded) subset $C \subset D$ such that:

$$\mu(D \setminus C) < \epsilon$$

and Φ_{solu} restricted to C is continuous:

$$\Phi_{\text{solu}}|_C : C \to \mathbb{R}^m \text{ is continuous.}$$

Since C is compact and $\Phi_{\text{solu}}|_C$ is continuous, the Universal Approximation Theorem ensures that there exists a neural network $F_{\text{HYA},W} \in \mathcal{F}_{\text{HYA},W}^{\text{MILPnet}}$ such that:

$$\sup_{x \in C} \|F_{\text{HYA},W}(x) - \Phi_{\text{solu}}(x)\| < \delta.$$

This implies that for all $x \in C$:

$$\|F_{\text{HYA},W}(x) - \Phi_{\text{solu}}(x)\| < \delta.$$

Consider the probability that the approximation error exceeds δ:

$$P\left(\|F_{\text{HYA},W}(x) - \Phi_{\text{solu}}(x)\| > \delta\right).$$

This event can only occur if $x \in D \setminus C$, since for $x \in C$, the error is guaranteed to be less than δ. Therefore:

$$P\left(\|F_{\text{HYA},W}(x) - \Phi_{\text{solu}}(x)\| > \delta\right) \leq \mu(D \setminus C) < \epsilon.$$

Thus, we have:

$$P\left(\|F_{\text{HYA},W}(x) - \Phi_{\text{solu}}(x)\| > \delta\right) < \epsilon.$$

By Lusin's Theorem, we ensure that Φ_{solu} is continuous on a large subset C of D. The Universal Approximation Theorem then guarantees the existence of a neural network $F_{\text{HYA},W}$ that approximates Φ_{solu} within δ on C. Consequently, the probability that the approximation error exceeds δ on the entire dataset D is bounded by ϵ.

This establishes that for infinite or continuous datasets with finite measure, there exists a neural network within $\mathcal{F}_{\text{HYA},V}^{\text{MILPnet}}$ that satisfies the desired probabilistic bound on the approximation error. □

H PROOF OF THE STABILITY

In this section, we establish the stability properties of the MILP mappings Φ_{feas}, Φ_{obj}, and Φ_{solu} under small perturbations of problem coefficients. Our analysis builds upon Berge's Maximum Theorem (Aliprantis & Border, 2006).

Theorem 19 (Berge's Maximum Theorem Aliprantis & Border (2006))**.** *Let X and T be topological spaces, and let $f : X \times T \to \mathbb{R}$ be continuous. Let $C : T \rightrightarrows X$ be a correspondence (set-valued map) such that:*

1. *$C(t)$ is non-empty and compact for all $t \in T$,*
2. *C is continuous, i.e., its graph $Gr(C) = \{(t, x) : x \in C(t)\}$ is closed and C is lower hemicontinuous.*

Define the value function and argmax correspondence by:

$$V(t) = \max_{x \in C(t)} f(x,t), \quad X^*(t) = \arg\max_{x \in C(t)} f(x,t) = \{x \in C(t) : f(x,t) = V(t)\}.$$

Then:

1. *$V(t)$ is continuous in t.*
2. *$X^*(t)$ is non-empty, compact-valued, and upper hemicontinuous in t.*

We first analyze the stability of Φ_{obj}, which exhibits the strongest stability properties among the three mappings.

Definition 20 (Continuous Relaxation for MILP sequence)**.** For a MILP sequence $\mathbf{x} = [h^1_{\text{cons}}, \ldots, h^m_{\text{cons}}, h^{i'}, h^{\ell'}, h^{\mathfrak{O}'}, h^{c'}] \in H^{\text{MILP}}$, its *continuous relaxation* is the linear program obtained by dropping the integrality constraints:

$$\text{CR}(\mathbf{x}): \quad \min_{x \in \mathbb{R}^n} \{\langle c, x\rangle : Ax \le b,\ \ell \le x \le u\},$$

where A, b, c, ℓ, u are extracted from the tokens in $\mathbf{x}$.

Proposition 21 (Stability of Continuous Relaxation)**.** Let $\mathbf{x} \in H^{\text{MILP}}$ be a feasible MILP instance whose continuous relaxation has a bounded feasible region. Then the optimal value function of the continuous relaxation, denoted $\Phi^{\text{CR}}_{\text{obj}}$, is continuous at $\mathbf{x}$. Furthermore, if the optimal solution is non-degenerate, then $\Phi^{\text{CR}}_{\text{obj}}$ is locally Lipschitz continuous with constant:

$$L = \|c\|_2 \cdot \text{diam}(\text{Feas}(\mathbf{x})),$$

where $\text{Feas}(\mathbf{x})$ denotes the feasible region and $\text{diam}(\cdot)$ its diameter.

Proof. The continuous relaxation defines a parametric linear program where the parameter $t = (A, b, c, \ell, u)$ lives in H^{MILP}. Let $X = \mathbb{R}^n$ and $T = H^{\text{MILP}}$. The objective function $f(x,t) = \langle c, x\rangle$ is continuous in (x,t). Then the feasible region correspondence $C(t) = \{x \in \mathbb{R}^n : Ax \le b, \ell \le x \le u\}$ satisfies:

- **Compactness:** By assumption, $C(\mathbf{x})$ is bounded. Combined with the closed constraints, $C(\mathbf{x})$ is compact.
- **Continuity:** The graph $\text{Gr}(C)$ is closed because the constraints define a closed set in $\mathbb{R}^n \times H^{\text{MILP}}$. Moreover, C is lower hemicontinuous: for any $x \in C(t)$ and $t_n \to t$, since the constraints are linear and continuous in t, small perturbations preserve feasibility in a neighborhood.

By Berge's Theorem 19, $\Phi^{\text{CR}}_{\text{obj}}(\mathbf{x})$ is continuous at $\mathbf{x}$. Under non-degeneracy, the optimal basis remains unchanged in a neighborhood of $\mathbf{x}$. The optimal value is given by the basis solution $x^* = B^{-1}b_B$, where B is the optimal basis matrix. The objective value is:

$$\Phi^{\text{CR}}_{\text{obj}}(\mathbf{x}) = \langle c_B, B^{-1}b_B\rangle,$$

which is a linear function of (c_B, b_B) within the neighborhood where the basis is constant.

For a perturbation $\mathbf{x}' = \mathbf{x} + \boldsymbol{\epsilon}$ with $\|\boldsymbol{\epsilon}\|_2 \le \delta$:

$$\begin{aligned}
|\Phi^{\text{CR}}_{\text{obj}}(\mathbf{x}') - \Phi^{\text{CR}}_{\text{obj}}(\mathbf{x})| &= |\langle c', x'^*\rangle - \langle c, x^*\rangle| \\
&\le |\langle c' - c, x'^*\rangle| + |\langle c, x'^* - x^*\rangle| \\
&\le \|c' - c\|_2 \cdot \|x'^*\|_2 + \|c\|_2 \cdot \|x'^* - x^*\|_2 \\
&\le L \cdot \delta,
\end{aligned}$$

where $L = \|c\|_2 \cdot \text{diam}(\text{Feas}(\mathbf{x}))$ bounds both terms. □

H.1 Stability of the Optimal Objective Mapping

Theorem 22 (Conditional Stability of MILP Objective Value). *Let $\mathbf{x} \in H^{MILP}$ be a feasible MILP sequence with bounded feasible region. Consider a perturbation $\mathbf{x}' = \mathbf{x} + \boldsymbol{\epsilon}$ where $\|\boldsymbol{\epsilon}\|_2 \leq \delta$. If the following assumptions hold:*

1. ***Feasibility preservation:*** $\Phi_{feas}(\mathbf{x}') = 1$,
2. ***Optimal solution stability:*** *The optimal integer solution $x^* \in \mathbb{Z}^n$ of $\mathbf{x}$ remains feasible for $\mathbf{x}'$,*
3. ***Bounded diameter:*** $diam(Feas(\mathbf{x}) \cap \mathbb{Z}^n) \leq D$,

then:

$$|\Phi_{obj}(\mathbf{x}') - \Phi_{obj}(\mathbf{x})| \leq (\|c\|_2 + \delta) \cdot D.$$

Proof. Let $x^* \in \mathbb{Z}^n$ be an optimal solution to $\mathbf{x}$, and $x'^* \in \mathbb{Z}^n$ be an optimal solution to $\mathbf{x}'$.

By condition (2), x^* is feasible for $\mathbf{x}'$, so:

$$\Phi_{\text{obj}}(\mathbf{x}') = \langle c', x'^* \rangle \leq \langle c', x^* \rangle.$$

Similarly, x'^* is feasible for its problem, and by condition (1), both x^* and x'^* lie in the bounded integer feasible region. Thus:

$$\Phi_{\text{obj}}(\mathbf{x}) = \langle c, x^* \rangle.$$

Now:

$$\begin{aligned}
|\Phi_{\text{obj}}(\mathbf{x}') - \Phi_{\text{obj}}(\mathbf{x})| &= |\langle c', x'^* \rangle - \langle c, x^* \rangle| \\
&\leq |\langle c', x'^* \rangle - \langle c, x'^* \rangle| + |\langle c, x'^* \rangle - \langle c, x^* \rangle| \\
&= |\langle c' - c, x'^* \rangle| + |\langle c, x'^* - x^* \rangle| \\
&\leq \|c' - c\|_2 \cdot \|x'^*\|_2 + \|c\|_2 \cdot \|x'^* - x^*\|_2 \\
&\leq \delta \cdot D + \|c\|_2 \cdot D \\
&= (\|c\|_2 + \delta) \cdot D,
\end{aligned}$$

where we used $\|c' - c\|_2 \leq \delta$ (from the perturbation bound) and $\|x'^* - x^*\|_2, \|x'^*\|_2 \leq D$ (from condition 3). □

H.2 Stability of the Feasibility Mapping

We now analyze the stability of Φ_{feas}.

Theorem 23 (Conditional Stability of Feasibility). *Let $\mathbf{x} \in H^{MILP}$ with $\Phi_{feas}(\mathbf{x}) = 1$. Suppose the feasible integer points satisfy a* strict feasibility *condition: there exists $\rho > 0$ such that for all $x^* \in Feas(\mathbf{x}) \cap \mathbb{Z}^n$,*

$$Ax^* \leq b - \rho\mathbf{1}, \quad \ell + \rho\mathbf{1} \leq x^* \leq u - \rho\mathbf{1},$$

where $\mathbf{1}$ is the all-ones vector. Then for any perturbation $\mathbf{x}' = \mathbf{x} + \boldsymbol{\epsilon}$ with $\|\boldsymbol{\epsilon}\|_\infty \leq \delta < \rho$, we have:

$$\Phi_{feas}(\mathbf{x}') = 1.$$

Proof. Let $x^* \in \text{Feas}(\mathbf{x}) \cap \mathbb{Z}^n$ be any feasible integer point for $\mathbf{x}$.

For the perturbed instance $\mathbf{x}'$ with parameters (A', b', ℓ', u'), we have:

$$\|A' - A\|_\infty \leq \delta, \quad |b'_i - b_i| \leq \delta, \quad |\ell'_j - \ell_j| \leq \delta, \quad |u'_j - u_j| \leq \delta.$$

Check constraint satisfaction:

$$\begin{aligned}
A'x^* &= (A + \Delta A)x^* = Ax^* + \Delta A x^* \\
&\leq (b - \rho\mathbf{1}) + \|\Delta A\|_\infty \|x^*\|_1 \mathbf{1} \\
&\leq b - \rho\mathbf{1} + \delta\|x^*\|_1 \mathbf{1}.
\end{aligned}$$

If $\delta < \frac{\rho}{\|x^*\|_1}$, then $A'x^* < b - (\rho - \delta\|x^*\|_1)\mathbf{1} < b'$.

For sufficiently small $\delta < \rho$, we can ensure all integer points remain strictly feasible. Therefore, $\Phi_{\text{feas}}(\mathbf{x}') = 1$. □

H.3 Stability of the Optimal Solution Mapping

Finally, we analyze Φ_{solu}.

Theorem 24 (Conditional Stability of Solution Mapping)**.** *Let $\mathbf{x} \in H^{MILP}$ with optimal solution $x^* \in \mathbb{Z}^n$. Suppose x^* is the* unique optimal solution *and satisfies a* strong optimality gap *condition: for all $x \in Feas(\mathbf{x}) \cap \mathbb{Z}^n$ with $x \neq x^*$,*

$$\langle c, x\rangle > \langle c, x^*\rangle + \gamma,$$

for some $\gamma > 0$. Then there exists $\delta > 0$ such that for any perturbation $\mathbf{x}' = \mathbf{x} + \boldsymbol{\epsilon}$ with $\|\boldsymbol{\epsilon}\|_2 \leq \delta$:

$$\Phi_{solu}(\mathbf{x}') = x^*.$$

That is, the optimal solution remains unchanged.

Proof. For the perturbed instance with objective $c' = c + \Delta c$ where $\|\Delta c\|_2 \leq \delta$:

For any $x \in \text{Feas}(\mathbf{x}') \cap \mathbb{Z}^n$ with $x \neq x^*$:

$$\begin{aligned}\langle c', x\rangle - \langle c', x^*\rangle &= \langle c + \Delta c, x\rangle - \langle c + \Delta c, x^*\rangle \\ &= (\langle c, x\rangle - \langle c, x^*\rangle) + \langle \Delta c, x - x^*\rangle \\ &\geq \gamma - \|\Delta c\|_2 \|x - x^*\|_2 \\ &\geq \gamma - \delta \cdot D,\end{aligned}$$

where $D = \max_{x \neq x^*} \|x - x^*\|_2$ over the finite integer feasible set. If $\delta < \frac{\gamma}{D}$, then $\langle c', x\rangle > \langle c', x^*\rangle$ for all $x \neq x^*$, ensuring x^* remains optimal for $\mathbf{x}'$. □

I Details of the Time-complexity of MILPnet

Excluding the linear transformation, the time complexity for multi-scale operations across all windows is $O\left(\sum_{k=1}^{N} h \cdot \eta_k^2\right)$. The global attention mechanism employs a global multi-head self-attention mechanism over the entire sequence, resulting in a final time complexity of $O\left(\sum_{k=1}^{N} h\eta_k^2 d + h(m+4)^2 d\right)$ for the hybrid attention. Given that the maximum window size satisfies $w_{\max} \leq m + 4$, it follows that $\sum_{k=1}^{N} \eta_k^2 \leq N \cdot (m+4)^2$. Therefore, the time complexity can be further simplified to $O\left(h \cdot (m+4)^2 d\,(N+1)\right)$, where d represents the linear embedding size and h denotes the number of attention heads.

J Sparse Variant

To mitigate the quadratic overhead of global attention, we evaluated a multi-scale sliding sparse attention (with sliding mask) to replace the global attention, and discovered that it can achieve faster inference while maintaining comparable performance. As the sparse sliding attention uses sparse masks to restrict each position's attention only to specific locations beyond the step interval s, the time complexity of the stride attention is:

$$\mathcal{T}_{\text{stride}} = \mathcal{O}\left(\frac{h(m+4)^2 d}{s}\right) \tag{23}$$

Thus, the time complexity of multi-scale sliding spare attention becomes:

$$\begin{aligned}\mathcal{T}_{\text{sparse}} &= \mathcal{O}(knwdh) + \mathcal{O}(n^2 dh/s) &(24)\\ &= \mathcal{O}(dh(k(m+4)w + (m+4)^2/s)) &(25)\end{aligned}$$

Table 14: Experimental results on FOLD(200,20) with 1-hour pre-training and a stride of 2

	Fold(200,20)		
	Error	Inference Time	MSE
GCN	5000	0.228	0.268
MILPnet(Sparse)	763	**0.033**	0.091
MILPnet(ours)	**191**	0.117	**0.016**

We can calculate the speed-up ratio against our original design as:

$$\text{Speedup} = \frac{Nw^2 + n^2}{Nw^2 + n^2/s} \tag{26}$$

In practice, $n^2 \gg Nw^2$ (sequence length is much larger than window size), so the speed-up of the time-complexity is finally as:

$$\text{Speedup} \approx \frac{n^2}{n^2/s} = \boxed{s}$$

This signifies that the model's scalability with engineering optimizations.

K Details of the Experiments

K.1 Detailed Experiment Settings

Baselines. As methods using variant GNNs for MILP representation are still limited, we adapted several representative graph algorithms to serve as baselines. To validate the advantages of our sequence-based algorithm, we compare our model against multiple graph-based representation methods that **model MILPs as bipartite graphs**. The **GNN-based networks** include GCN (Chen et al., 2023b), GIN (Xu et al., 2019), and SAGE (Wu et al., 2021). The attention-based graph networks include PGN (Cappart et al., 2022) and GraphGPS (Wang et al., 2023b). We also include the **random feature graph modeling method** proposed in (Chen et al., 2023b), which is specifically designed to alleviate the feasibility prediction problem on Foldable instances.

Metrics. We established several evaluation metrics for the experimental settings of the various feature mappings discussed in the context of Mixed-Integer Linear Programming (MILP). (1)**Approximation Error**: For all feature mappings, we assessed the average approximation error, defined as the mean of prediction errors across all instances. (2) **Feasibility Error Number**: Specifically for feasibility mappings, we designed metrics to measure the error prediction rate and the number of prediction errors. (3)**Model Params**: We evaluated the size of the model parameters to assess the impact of different feature mappings on the model's complexity.

Implementation. The MILPnet module is implemented using PyTorch. Our experiments were conducted on a single NVIDIA 4090Ti GPU (24GB) and a 12th Gen Intel(R) Core(TM) i5-12600KF 3.69GHz CPU.

K.2 Details of Generating Foldable MILP instances

We follow the foldable dataset generation method in (Chen et al., 2023a), and set the $c_1 = \cdots = c_n = 0$ foldable instances as D1, the $c_1 = \cdots = c_n = 0.01$ foldable instances as D2. We use D1 and D2 as our experimental datasets. It is worth mentioning that in the representation and generalization experiments on foldable instances, our training set contains 10,000 foldable instances, while the test set also includes 10,000 foldable instances, with each set containing 5,000 feasible instances. It is worth mentioning that Chen et al.'s dataset construction was only performed on FOLD(20,6), whereas we have extended it to dataset constructions on sizes FOLD(m,n).

Variable Generation: The lower and upper bounds for each variable x_j are generated from a normal distribution. If the lower bound is greater than the upper bound, they are swapped. Some variables are specified as integer variables (i.e., $x_j \in \{0, 1\}$), while others are continuous variables.

Feasible and Infeasible Problem Constraint Setup: For the feasible problem ($k1$), the constraints are set as follows:

$$x_{j_1} + x_{j_2} = 1, \quad x_{j_2} + x_{j_3} = 1, \quad \ldots, \quad x_{j_n} + x_{j_1} = 1$$

These constraints connect binary variables with equality, forming a cyclic structure that guarantees the problem is feasible; For the infeasible problem ($k2$), the constraints are slightly adjusted to make the problem infeasible. For example:

$$x_{j_1} + x_{j_2} = 1, \quad x_{j_2} + x_{j_3} = 1, \quad x_{j_3} + x_{j_1} = 1$$

This setup results in an infeasible problem.

K.3 Details of the Representation experiments

In the representation experiments of our MILPnet on Foldable instances, the MILPnet consists of 1 layer. The embedding dimension is 216 or 256. The learning rate is set to 0.0001, the seeds are chosen from 42 or 0. The graph-based methods share the same set of experimental seeds as MILPnet. And our feasibility dataset consists of 50% feasible instances and 50% infeasible instances, while other datasets are obtained by removing infeasible samples.

K.4 Details of the Generalization Experiments

In the generalization experiments of our MILPnet on Foldable instances, the network parameters pre-trained on the training set are the same as those used in the representation experiments. For the feasibility generalization experiments, we limited the pre-training time, setting it to 3 minutes and 5 minutes on FOLD20, 10 minutes and 30 minutes on FOLD50, and 1 hours on FOLD100 to FOLD500. We then compared the performance of our model with other baselines under different pre-training time constraints. For the optimal solution and objective optimal value generalization experiments, we set the pre-training time of FOLD20 to 10 minutes and FOLD50 to 60 minutes. For our MILPnet generalization experiments, we chose our dropout rate from $\{0.3, 0.5\}$, the max window size is chosen from $\{2, 3, 4, 5\}$, and the number of the MILPnet block is 1.

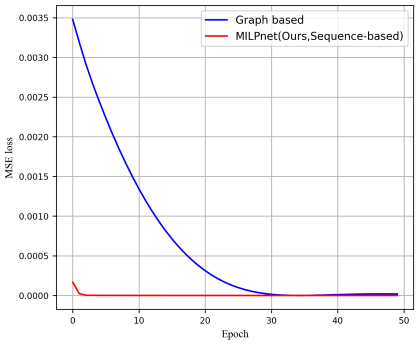

Figure 15: Representation experiments on the optimal objective value for FOLD20. MILPnet approximates the optimal value mapping of Foldable MILP instances with smaller errors than graph-based method.

K.5 Four Common Real-World MILP solving benchmarks

This section introduces the details of constructing specific MILP instances. In particular, for the SC, CA, and FC problems, we follow the instance construction method described in Learn2Branch (Gasse et al., 2019), and the numbers of variables and constraints are shown in the table below. Meanwhile, for the SC problem, the density is set to 0.05; and for the FC problem, the ratio is also set to 5.

Table 15: Number of variables and constraints for real-world benchmarks

Dataset	Variables	Constraints
IP	1,083	195
SC	200	40
CA	300	40
FC	200	60

L ADDITIONAL UNFOLDABLE EXPERIMENTS.

Although this paper primarily conducts experiments on foldable MILP instances, we also perform representation experiments on unfoldable instances. Similarly, we compare our method with graph-based networks. In this part, the max window size is chosen as 2, and the MILPnet embedding size is chosen as 32, the graph-based methods (We select GCN) embedding size is 8.

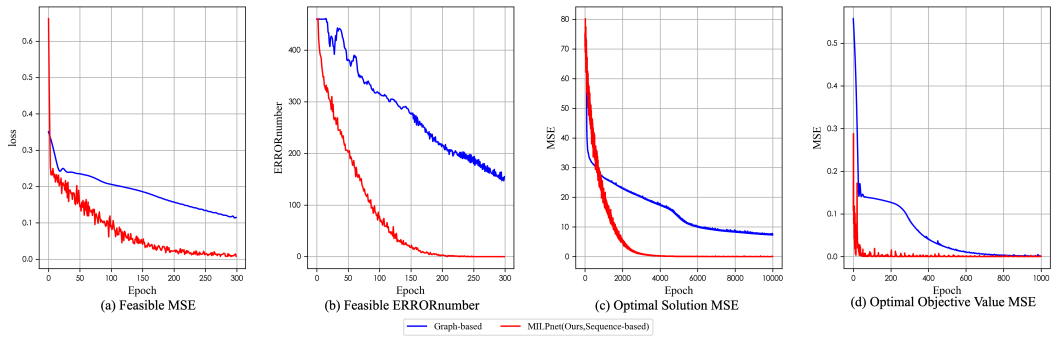

Figure 16: In the representation experiments on unfold20, MILPnet still outperforms graph-based methods with a smaller approximation error. Additionally, it maintains a smaller parameter size while achieving an estimation error lower than that of the graph-based method.